The Astrophysical Journal, 966:133 (18pp), 2024 May 1 https://doi.org/10.3847/1538-4357/ad2e93

Constraints on the $z \sim 5$ Star-forming Galaxy Luminosity Function From Hubble Space Telescope Imaging of an Unbiased and Complete Sample of Long Gamma-Ray Burst Host Galaxies

Huei Sears[1,2], Ryan Chornock[3], Jay Strader[4], Daniel A. Perley[5], Peter K. Blanchard[1,2], Raffaella Margutti[3,6], and Nial R. Tanvir[7]

[1] Center for Interdisciplinary Exploration and Research in Astrophysics (CIERA), Northwestern University, Evanston, IL 60202, USA
[2] Department of Physics and Astronomy, Northwestern University, Evanston, IL 60208, USA
[3] Department of Astronomy, University of California, Berkeley, CA 94720-3411, USA
[4] Center for Data Intensive and Time Domain Astronomy, Department of Physics and Astronomy, Michigan State University, East Lansing, MI, USA
[5] Astrophysics Research Institute, Liverpool John Moores University, Liverpool Science Park, 146 Brownlow Hill, Liverpool L3 5RF, UK
[6] Department of Physics, University of California, 366 Physics North MC 7300, Berkeley, CA 94720, USA
[7] School of Physics and Astronomy, University of Leicester, University Road, Leicester LE1 7RH, UK
Received 2023 August 27; revised 2024 February 25; accepted 2024 February 27; published 2024 April 30

Abstract

We present rest-frame UV Hubble Space Telescope imaging of the largest and most complete sample of 23 long-duration gamma-ray burst (GRB) host galaxies between redshifts 4 and 6. Of these 23, we present new WFC3/F110W imaging for 19 of the hosts, which we combine with archival WFC3/F110W and WFC3/F140W imaging for the remaining four. We use the photometry of the host galaxies from this sample to characterize both the rest-frame UV luminosity function (LF) and the size–luminosity relation of the sample. We find that when assuming the standard Schechter-function parameterization for the UV LF, the GRB host sample is best fit with $\alpha = -1.30^{+0.30}_{-0.25}$ and $M_* = -20.33^{+0.44}_{-0.54}$ mag, which are consistent with results based on $z \sim 5$ Lyman-break galaxies. We find that ∼68% of our size–luminosity measurements fall within or below the same relation for Lyman-break galaxies at $z \sim 4$. This study observationally confirms expectations that at $z \sim 5$ Lyman-break and GRB host galaxies should trace the same population and demonstrates the utility of GRBs as probes of hidden star formation in the high-redshift Universe. Under the assumption that GRBs unbiasedly trace star formation at this redshift, our nondetection fraction of 7/23 is consistent at the 95% confidence level with 13%–53% of star formation at redshift $z \sim 5$ occurring in galaxies fainter than our detection limit of $M_{1600\text{Å}} \approx -18.3$ mag.

Unified Astronomy Thesaurus concepts: Gamma-ray bursts (629); High-redshift galaxies (734); Galaxies (573)

1. Introduction

Long-duration gamma-ray bursts (GRBs) have been theoretically (Paczynski 1986; Woosley 1993) and observationally associated with the deaths of massive stars and specifically with Type Ib/c broad-lined (BL) supernovae (SNe). These SNe result from the core collapse of a progenitor star that has completely lost its hydrogen shell and most-to-all of its helium shell, with the "BL" designation in reference to the fast moving SN ejecta resulting in BL emission features (Galama et al. 1998; MacFadyen & Woosley 1999; Hjorth et al. 2003; see Woosley & Bloom 2006; Hjorth & Bloom 2012; Cano et al. 2017 for reviews).[8]

There are two main observational components to a GRB—the initial gamma-ray prompt emission is thought to be from dissipation processes within the GRB jet and the multi-wavelength afterglow powered by the synchrotron emission originating from the jet's deceleration into the local environment (Chevalier & Li 1999; Miceli & Nava 2022).

GRB follow-up and afterglow studies were revolutionized with the launch of the Neil Gehrels Swift Observatory (Swift; Gehrels et al. 2004). The X-ray Telescope (XRT; Burrows et al. 2005) on board has the ability to localize the GRB afterglow to few arcsecond precision allowing for groundbased observations. As long-duration GRBs are known to occur predominantly within the half-light radius and within the bright, star-forming regions of their host galaxies (Fruchter et al. 2006; Svensson et al. 2010; Blanchard & Berger 2016; Lyman et al. 2017), this precise afterglow-enabled localization often allows for robust host identification. The extreme luminosity ($\sim 10^{53}$ erg s^{-1}) of the GRB makes them observable to cosmological distances, with the currently most distant GRB 090429B photometrically estimated to have $z = 9.4$ (Cucchiara et al. 2011).

High-redshift ($z > 3$) star-forming galaxies are primarily identified using the Lyman-break technique in which the wavelength of the Lyman break is determined via photometric dropout (Steidel et al. 1996). Studies of star-forming galaxies benefit from large-number statistics and deep observations and, prior to JWST, extend through $z \sim 9$ (see, e.g., Stark 2016 for a recent review). Surveys from JWST, including early data release and dedicated programs like the Cosmic Evolution Early Release Science Survey (CEERS; Finkelstein et al. 2023), the GLASS JWST Early Release Science Program (GLASS-JWST; Treu et al. 2022), and the JWST Advanced Deep Extragalactic Survey (JADES; Eisenstein et al. 2023)

[8] There have been a handful of long GRBs identified to likely be associated with compact object mergers, e.g., GRBs 230307A (Gillanders et al. 2023; Levan et al. 2024), 211211A (Rastinejad et al. 2022; Troja et al. 2022; Gompertz et al. 2023), and 060614 (Fynbo et al. 2006b; Della Valle et al. 2006; Gal-Yam et al. 2006; Gehrels et al. 2006). At early cosmic times, however, the contamination of bright long-GRB samples by merger events is likely to be minimal.

have allowed for analysis of these galaxies to continue to even greater redshift ($z \sim 13$). An important characterization of Lyman-break galaxies is the UV luminosity function (LF). This function is a fit to a histogram of these galaxies and allows for an estimate of the percentage of undetectable star formation through extrapolation of the fit to faint magnitudes, whether intrinsic or the consequence of dust obscuration. It is well defined at the bright end ($M_{\rm UV} < -15$ mag; Finkelstein et al. 2015; Bouwens et al. 2021, 2022a; Finkelstein et al. 2023; Harikane et al. 2023, 2024) with the generally assumed Schechter (1976) function being fit to measurements from thousands of galaxies.

Observations of Lyman-break galaxies, however, only offer a view of the star formation that can be directly observed and are therefore implicitly biased against faint galaxies. Since the ability to detect a GRB is independent of the luminosity of its host galaxy, and the detection of a GRB implies the existence of a galaxy at that location, GRBs offer a way to characterize faint and otherwise unobserved star formation, such as that which is dust obscured or intrinsically faint. Constraining the amount of star formation that would otherwise go undetected, especially at high redshift, is key for determining how large a role this star formation played in reionizing the Universe.

In the low-redshift Universe ($z < 2$) GRB host galaxies have been shown to have smaller sizes, lower masses, and lower metallicities than the general star-forming galaxy population (Stanek et al. 2006; Kewley et al. 2007; Han et al. 2010; Levesque et al. 2010; Svensson et al. 2010; Graham & Fruchter 2013; Perley et al. 2013; Palmerio et al. 2019). These biases are thought to be a consequence of the preference for a GRB progenitor to form and explode in low-metallicity environments, with low-metallicity star-forming galaxies being smaller and less massive than the general sample (Mannucci et al. 2010; Palmerio et al. 2019). The nature of this preference, both physical and functional, is still actively debated: some studies have theorized multiple metallicity-dependent paths for GRB creation (Trenti et al. 2015; hereafter T15), while some have found evidence for a host galaxy stellar metallicity threshold above which GRBs are rare (i.e., it allows for the possibility of a pocket of lower-Z star formation within a high-Z galaxy). Below this threshold, GRBs seem to trace star formation in an unbiased way (though there is uncertainty on the value of this threshold ($Z < Z_{\odot}$: Perley et al. 2016b; $Z < 0.7Z_{\odot}$: Palmerio et al. 2019).

The bias of the GRBs in host galaxy mass and size is consistent with being largely a by-product of metal aversion (Perley et al. 2016b), and so, as the average metallicity of the Universe decreases with increasing redshift, the differences in the characteristics of GRB host galaxies as compared to those of actively star-forming galaxies should decrease toward triviality. Indeed, up to $z \sim 4$, comparisons of the two galaxy samples have followed this expectation when characterized by the mass–metallicity relation (Levesque et al. 2010; Laskar et al. 2011; Vergani et al. 2017; Graham et al. 2023), the UV LF (Greiner et al. 2015; Schulze et al. 2015), and in direct size and stellar mass measurements (Vergani et al. 2015; Schneider et al. 2022). Comparisons at higher redshift ($z \sim 6$) also support these results but are significantly limited in precision due to the small number of localized GRBs with confirmed redshifts at this redshift range (Tanvir et al. 2012a; McGuire et al. 2016).

In this work, we present new Hubble Space Telescope (HST) observations of the largest complete sample of GRB host galaxies at $z \sim 5$, to improve significantly these comparisons at the highest possible redshifts with currently available data. In Section 2, we describe our observations and host identification methods. We present our formalism, modeling, and analysis of the UV LF and size–luminosity relation of the GRB host sample and compare to that of Lyman-break galaxies in Section 3. We conclude with a presentation and discussion of our nondetection fraction and its implications toward the amount of undetectable star formation. We use a cosmological model with $H_0 = 70$ km s^{-1} Mpc^{-1}, $\Omega_0 = 0.3$, and $\Omega_\Lambda = 0.7$. Uncertainties are reported as the Gaussian-equivalent 1σ, unless otherwise stated.

2. Observations

2.1. Sample Selection

We define selection criteria for our $z \sim 5$ GRB host galaxy sample to minimize selection bias while maximizing completeness. Our initial selection criteria were:

1. the GRB has a spectroscopic or photometric redshift of $4 < z < 6$;
2. deep observations at the GRB location were performed with the Spitzer Space Telescope (Spitzer; Werner et al. 2004);
3. the GRB was detected with Swift prior to mid-2015 (the date is a by-product of the Spitzer requirement) and has a localization $\leqslant 2''$; and
4. the line of sight along the GRB direction has low Galactic extinction, $E(B-V) < 0.2$ mag.

From this first-round sample, we use the following criteria to determine the final sample:

1. the GRB was included in one of the four following uniform samples: The Optically Unbiased GRB Host Survey (TOUGH; Schulze et al. 2015), A Complete Sample of Bright Swift Long Gamma-Ray Bursts (BAT6; Salvaterra et al. 2012), the X-shooter GRB afterglow legacy sample (XSGRB; Selsing et al. 2019), or the Swift GRB Host Galaxy Legacy Survey (SHOALS; Perley et al. 2016a), or otherwise met the criteria to be included in the SHOALS sample but occurred outside of the project timeline, or
2. the GRB was rapidly observed with a near-infrared (NIR) imager on a >1 m telescope, such as the Palomar 60 inch Telescope (P60; Cenko et al. 2006), the Peters Automated Infrared Imaging Telescope (PAIRITEL; Bloom et al. 2006), or the Gamma-Ray Burst Optical/Near-Infrared Detector (GROND; Greiner et al. 2008) on the MPG/ESO 2.2 m telescope.

While the Spitzer observations are not used in our analysis, the existence of these Spitzer images helped us to rule out low-redshift interlopers and, in a few cases for which there was not a spectroscopic redshift measurement, allowed us to measure photometric redshifts, though these measurements were already published in samples such as SHOALS (Perley et al. 2016a). Of the 31 host galaxies identified by the redshift and time cuts, only five of these do not have Spitzer imaging. These five sources would have otherwise been excluded from our sample

due to our localization, Galactic extinction, and inclusion in a uniform sample criteria.

The typical accuracy of Swift/XRT (with the enhanced analysis) is $\sim 1\farcs5$ (Goad et al. 2007). This is an algorithm update (Goad et al. 2007; Evans et al. 2009) and not a physical update to the instrument, and so this accuracy is applicable to all bursts with observations from Swift/XRT and the Ultraviolet and Optical Telescope (UVOT; Roming et al. 2005) on board Swift; e.g., GRB 050505 was published with a $6''$ XRT positional uncertainty (Kennea et al. 2005) in 2005, however, it now has a $1\farcs4$ uncertainty listed in the Swift catalog (Evans et al. 2009). This uncertainty is only significantly worse when the afterglow is faint (and thereby sensitive to field and atmospheric conditions) or observations of the afterglow are delayed—properties unrelated to the host environment. If the afterglow is bright, and especially if it is detected with Swift/UVOT, it is not common for observations of the afterglow to be delayed. Typical accuracies for GRB afterglows are $0\farcs1$–$1''$ (optical/NIR from the ground), $0\farcs5$–$1''$ (UVOT; Goad et al. 2007), and $\sim 1\farcs5$ (XRT; Goad et al. 2007). All of these accuracies are less than our required $\leqslant 2''$ positional uncertainty, and so this criterion does not substantially limit in size nor bias our host sample.

Our conditional requirement of rapid NIR imaging represents the uniformity of NIR follow up. The programs through which the GRBs were rapidly imaged with NIR instruments were designed to follow up every GRB that was observable with the telescope, such as those listed in criterion 2. The sample of GRB host galaxies with rapid NIR follow up of the burst is therefore uniform in that the criteria for NIR follow up were exclusively based on characteristics unrelated to the properties of the host galaxy, such as the local weather, decl., and Sun angle.

From these criteria, we populate a sample of 19 GRBs for host galaxy follow up. There are four additional GRBs (050505, 060223A, 140304A, and 140311A) that meet our initial selection criteria that also have available HST imaging. After investigating the selection criteria for each of the uniform samples, these four GRBs had been excluded due to a small Sun hour angle separation, too high of a decl., were not observed with XRT within 10 minutes of the Swift Burst Alert Telescope (BAT; Barthelmy et al. 2005) trigger, or had too low a fluence ($S_{15-150\,\mathrm{keV}}$). These properties, as well as the nonexistence of rapid NIR follow up, have no dependence on the characteristics of the GRB host galaxy and therefore the inclusion of these four GRBs has no effect on the uniformity of our GRB host galaxy sample, and so we include them in our analysis to increase the sample size.

2.2. HST Imaging

We present new HST/WFC3 IR imaging for 19 galaxies in our sample (ID: 15644, PI: Perley), while the remaining four (GRBs 050505, 060223A, 140304A, and 140311A) had archival imaging available, which we detail in the following section. The 19 host galaxies from our program were imaged using the F110W filter: galaxies with redshift $z < 4.8$ were observed over two orbits (average exposure time of 4900 s), while those with $z > 4.8$ were observed over three orbits (average exposure time of 7400 s). Across our redshift range, the central rest-frame wavelength of F110W converts to 1650–2260 Å, which samples the rest-frame UV emission.

We use archival imaging for four sources which were previously observed by HST. The host galaxies of GRBs 060223, 060522, and 060927 were also imaged using WFC3/F110W (ID: 11734, PI: Levan) with three orbits for the fields of GRBs 060223 and 060522 and five orbits for the field of GRB 060927. The host of GRB 130606A was imaged using WFC3/F140W (ID: 13831, PI: Tanvir) over four orbits. At a redshift of $z = 5.913$ (Lunnan et al. 2013), the central wavelength of F140W translates to 2014 Å, which is comparable to the observations of the other objects in the sample.

The reduced (i.e., flat-fielded, charge-transfer-efficiency (CTE) corrected, dark-subtracted) and ICRS aligned HST images were downloaded from the Barbara A. Milkulski Archive for Space Telescopes (MAST; see Chapters 2 and 3 of Sahu 2021 for details on this reduction). To drizzle the HST frames and achieve a resolution past the instrument limitation, we use `Astrodrizzle` (Gonzaga et al. 2012) with `final_pixfrac` = 0.8 and `final_scale` = 0.065 for consistency with previous GRB host galaxy HST analyses (e.g., Blanchard & Berger 2016).

2.3. Afterglow Localizations

Our analysis requires robust and accurate GRB localizations in order to identify the host galaxy of each GRB, and for that purpose, when possible, we use imaging of the optical afterglow. We were able to use optical afterglow imaging for all but three sources in our sample. For these three sources with no optical/NIR afterglow imaging available, we use their position as reported from Swift-XRT (GRBs 050803 and 050922B; Goad et al. 2007) or from the Karl G. Jansky Very Large Array (VLA; Perley et al. 2011; GRB 140304A; Laskar et al. 2014).

Optical afterglow images were collected from the public archives of the Low Resolution Imaging Spectrometer at the W.M. Keck Observatory (Keck-LRIS; Oke et al. 1995), the Gemini-North/South Multi-Object Spectrograph at the Gemini-North/South Observatory (GMOS-N/S; Hook et al. 2004), the P60 at Palomar Observatory (Cenko et al. 2006), the Very Large Telescope (VLT), the Rapid Eye Mount (REM[9]) Telescope at La Silla Observatory, the Device Optimized for the LOw RESolution (DOLORES, in short LRS[10]) at the Telescopio Nazionale Galileo (TNG), and Swift/UVOT. To reduce images from Keck-LRIS, we use the `LPIPE` pipeline (Perley 2019). When possible, we use the reduction pipelines embedded within the archive services. We otherwise use standard reduction steps such as flat division, bias subtraction, and image stacking. Centroid positions for each afterglow were measured using `Source Extractor` (Bertin & Arnouts 1996). Imaging and reduction steps for each GRB afterglow are detailed in the Appendix with additional references in Table 1.

2.4. Astrometric Alignment

Many of the afterglow images had an initial world coordinate system (WCS) assigned by the data archive. For those that did not, we upload the afterglow image to Astrometry.net (Lang et al. 2010) to get a preliminary WCS assignment. To align the

[9] https://www.eso.org/public/teles-instr/lasilla/rem/
[10] https://www.tng.iac.es/instruments/lrs/

Table 1
List of GRBs in Our Sample and Their Afterglow Localizations

GRB	R.A. (ICRS, J2000)	Decl. (ICRS, J2000)	1σ Unc. ($''$)	Redshift	Imaging Source	Filter	Date of Imaging	References
050502B	9:30:10.0703	+16:59:47.177	0.060	$5.2^{+0.3}_{-0.3}$	TNG	*I*	2005 Mar 03	Afonso et al. (2011)
050505	09:27:03.2887	+30:16:23.907	0.050	4.275	Keck/LRIS	*I*	2005 Mar 06	Cenko et al. (2005)
050803[a]	23:22:37.84	+05:47:08.4	1.4	$4.3^{+0.60}_{-2.40}$	Swift/XRT	⋯	⋯	Goad et al. (2007)
050814	17:36:45.3814	+46:20:21.562	0.257	$5.77^{+0.12}_{-0.12}$	P60	*i*	2005 Aug 15	Cenko (2005)
050922B[a]	00:23:13.37	−05:36:17.3	2	$4.9^{+0.3}_{-0.6}$	Swift/XRT	⋯	⋯	Goad et al. (2007)
060206	13:31:43.4556	+35:03:03.186	0.067	4.059	P60	Clear	2006 Feb 06	Ofek et al. (2006)
060223	03:40:49.5661	−17:07:48.357	0.077	4.406	Swift/UVOT	*V*	2006 Feb 23	Blustin et al. (2006)
060510B	15:56:29.6236	+78:34:12.102	0.094	4.942	Gemini/GMOS-N	*i*	2006 May 10	Price et al. (2007)
060522	21:31:44.8367	+02:53:09.607	0.054	5.11	TNG	*R*	2006 May 22	D'Avanzo & Cummings (2006)
060927	21:58:11.9907	+05:21:48.355	0.128	5.467	VLT/FORS2	*I*	2006 Sep 30	Ruiz-Velasco et al. (2007)
071025	23:40:17.0849	+31:46:42.857	0.263	$4.8^{+0.4}_{-0.4}$	REM	*H*	2007 Oct 25	Covino et al. (2007)
090516A	09:13:02.5973	−11:51:15.055	0.023	4.111	VLT/FORS2	*R*	2009 May 17	de Ugarte Postigo et al. (2009)
100219A	10:16:48.4822	−12:34:00.587	0.036	4.667	Gemini/GMOS-S	*r*	2010 Feb 20	Cenko et al. (2010a)
100513A	11:18:26.8480	+03:37:39.899	0.022	4.772	Gemini/GMOS-N	*i*	2010 May 13	Cenko et al. (2010b)
111008A	04:01:48.2508	−32:42:33.260	0.080	4.99	Gemini/GMOS-S	*R*	2011 Oct 09	Levan et al. (2011)
120712A	11:18:21.2254	−20:02:01.292	0.058	4.175	Gemini/GMOS-S	*R*	2012 Jul 12	Tanvir et al. (2012b)
130606A	16:37:35.1301	+29:47:46.538	0.026	5.913	Gemini/GMOS-N	*i*	2013 Jun 07	Chornock et al. (2013)
131117A	22:09:19.3354	−31:45:44.477	0.084	4.042	VLT/X-Shooter	*R*	2013 Nov 17	Hartoog et al. (2013)
140304A[a]	02:02:34.17	+33:28:26.01	0.02	5.283	VLA	⋯	⋯	Laskar et al. (2014)
140311A	13:57:13.2771	+00:38:31.388	0.060	4.954	Gemini/GMOS-N	*i*	2014 Mar 12	Chornock et al. (2014b)
140428A	12:57:28.4075	+28:23:06.280	0.066	$4.68^{+0.52}_{-0.18}$	Keck/LRIS	*I*	2014 Apr 29	Perley (2014)
140518A	15:09:00.6009	+42:25:05.886	0.046	4.7055	Gemini/GMOS-N	*i*	2014 May 18	Chornock et al. (2014a)
140614A	15:24:40.4961	−79:07:43.255	0.349	4.233	VLT/X-Shooter	*i*'	2014 Jun 14	Kruehler et al. (2014)

Notes. From left to right: GRB name, position and uncertainty of the afterglow (as measured from afterglow imaging or reported in the literature), redshift of the afterglow, filter of the afterglow imaging, and references for the afterglow images (or reported position). Afterglow redshift citations are in the Appendix.
[a] Positions for these afterglows are reported from the literature.

afterglow images to the HST images, we used TweakReg (Gonzaga et al. 2012). In the first alignment attempt, we use a catalog of Gaia sources within 2′ of the afterglow position. If this failed or if there were fewer than six catalog sources in the HST image, we instead used a catalog of at least six, but often >10, matching sources (all of the bright and unsaturated stars and sometimes bright galaxies) between each afterglow and HST image pair. These sources were selected from visual inspection in SAOImageDS9 (DS9; Joye & Mandel 2003). The alignment was deemed successful when common sources were aligned to within approximately 1 HST pixel = 0.″065. In the case of GRB 060223, there was only one source (a saturated star) in common between the two images, and so we instead aligned each image separately to the Gaia DR2 catalog. Details on alignment steps for each source are in the Appendix.

The afterglow positions found by Source Extractor were then converted from pixel to WCS coordinates for use in host galaxy identification in the corresponding HST image. To quantify the uncertainty on the position of the afterglow, reported in Table 1, we add in quadrature the uncertainty in the afterglow centroid from Source Extractor and the rms of the astrometric match to the HST image of the host. When optical afterglow imaging was unavailable, we list the uncertainty reported in the literature (GRB 140304A; Laskar et al. 2014) or the Swift-XRT catalog (GRBs 050803 and 050922B; Goad et al. 2007). All but two afterglows (GRBs 050803 and 050922B, for which only Swift-XRT imaging was available) were localized to better than 0.″5, with a median localization uncertainty ∼ 0.″06.

For all but one case (GRB 050922B), if there was a galaxy coincident within the afterglow uncertainty region, we designate that as the host of the GRB, as lower-redshift GRB afterglows are found near the centers of their host galaxy (Blanchard & Berger 2016). Within the afterglow uncertainty region of GRB 050922B, there are two galaxies: a compact source and a merging system. In agreement with Perley et al. (2016a), we designate the merging system as the host of this GRB. The identification of this galaxy as the host is elaborated upon in the next section. If there was no galaxy within the region, we classified this as a nondetection for the host galaxy. Details on the detection classification for each host are in the Appendix, and excerpts of the HST imaging with afterglow positions, their 3σ uncertainty regions, and host galaxy identifications are shown in Figure 1.

2.5. P_{cc} Calculations

We consider the false alarm probability for our claimed host galaxies and nearby sources to our claimed nondetections. The false alarm probability is the chance of an unrelated galaxy being within the measured proximity to the line of sight to the GRB. When the afterglow is well localized, this probability is largely dependent on the offset from the afterglow and the apparent magnitude of the putative host. We calculate the probability of chance coincidence (P_{cc}) following the methods in Bloom et al. (2002) and using $P_{cc} = 1 - e^{-\pi \times R_e^2 \times \sigma(\leqslant m)}$. R_e is taken to be the maximum of $[3\sqrt{\sigma_{TIE}^2 + \sigma_{AG}^2}, \sqrt{R^2 + 4 \times R_{eff}^2}]$, where σ_{TIE} is the uncertainty in the astrometric tie between the afterglow and galaxy positions and σ_{AG} is the uncertainty in the afterglow position. R is the offset of the considered galaxy from the center of the afterglow, and R_{eff} is the half-light radius of this considered galaxy. $\sigma(\leqslant m)$ is calculated from summing the galaxy number densities below the measured m_{F110W} in Tables 3 and 4 in Metcalfe et al. (2006).

For our detections, we calculate the P_{cc} for the putative host. Only four of the 16 putative host galaxies had $P_{cc} > 0.1$. These were the host galaxies of GRBs 050803 ($P_{cc} = 0.98$), 050922B ($P_{cc} = 0.99$), 071025 ($P_{cc} = 0.12$), and 140614A ($P_{cc} = 0.21$). These four cases include our two GRBs with only Swift-XRT positions available (GRBs 050803 and 050922B) and two sources with the next largest afterglow positional uncertainty. In the cases of GRBs 050803 and 050922B, these GRBs were included in our sample due to the photometric redshifts of the claimed host galaxies (Perley et al. 2016a), and so we continue analysis with the assumption that these are the host galaxies of these GRBs. We repeated our analysis in Section 3 treating these hosts as nondetections, and found that the best-fit LF parameters are consistent to within 1σ, so our results are not strongly sensitive to the uncertainty in these host associations. In the other two cases, these were the only sources within the afterglow uncertainty region, and so we classify them as the host galaxy of their respective GRB. Details on each P_{cc} are in the Appendix.

For our nondetections, we calculate the P_{cc} for all sources detected by Source Extractor within a $5'' \times 5''$ box centered on the afterglow position reported in Table 1. Only two of the 21 nearby sources in the 5″ fields of our nondetections had $P_{cc} < 0.1$. These two sources (one each in the fields of GRBs 060927 and 100219A) were confirmed to have a lower redshift than each respective GRB and are therefore not the host galaxies. The galaxy in the field of GRB 060927 was detected in R-band VLT imaging (Basa et al. 2012) and has a redshift $z < 4$, which is incompatible with the spectroscopic afterglow redshift of $z = 5.467$ reported in Ruiz-Velasco et al. (2007). The galaxy in the field of GRB 100219A was spectroscopically confirmed to have $z = 0.217$ in Cenko et al. (2010a), which is incompatible with the spectroscopic afterglow redshift of $z = 4.667$ for GRB 100219A (Selsing et al. 2019). Because all other detected candidate host galaxies have $P_{cc} > 0.1$, we report the host galaxies of these seven GRBs as nondetections. Details on each P_{cc} are in Appendix.

2.6. HST Photometry

We measure apparent magnitudes of all detected GRB host galaxies with Source Extractor using MAG_AUTO with PHOT_AUTOPARAMS set to the default values of 2.5 and 3.5. This parameter couplet sets the multiplicative factor and minimum Kron radius used in the "auto" measurement and is explained in greater detail in the Source Extractor documentation.[11] These measurements are reported in Table 2. We convert these apparent magnitudes to absolute UV magnitudes at 1600 Å using the distance modulus and a K-correction, as detailed below. We first aperture correct the apparent magnitudes using the Encircled Energy (EE) tables from STScI.[12] We interpolate the table values for F110W and F140W with a cubic spline to determine the appropriate EE term for the precise KRON_RADIUS used by Source Extractor for each galaxy. We then correct these aperture-corrected magnitudes for Galactic dust absorption as reported in the NASA/IPAC Extragalactic Database (NED;

[11] https://sextractor.readthedocs.io/en/latest/Photom.html

[12] https://www.stsci.edu/hst/instrumentation/wfc3/data-analysis/photometric-calibration/ir-encircled-energy

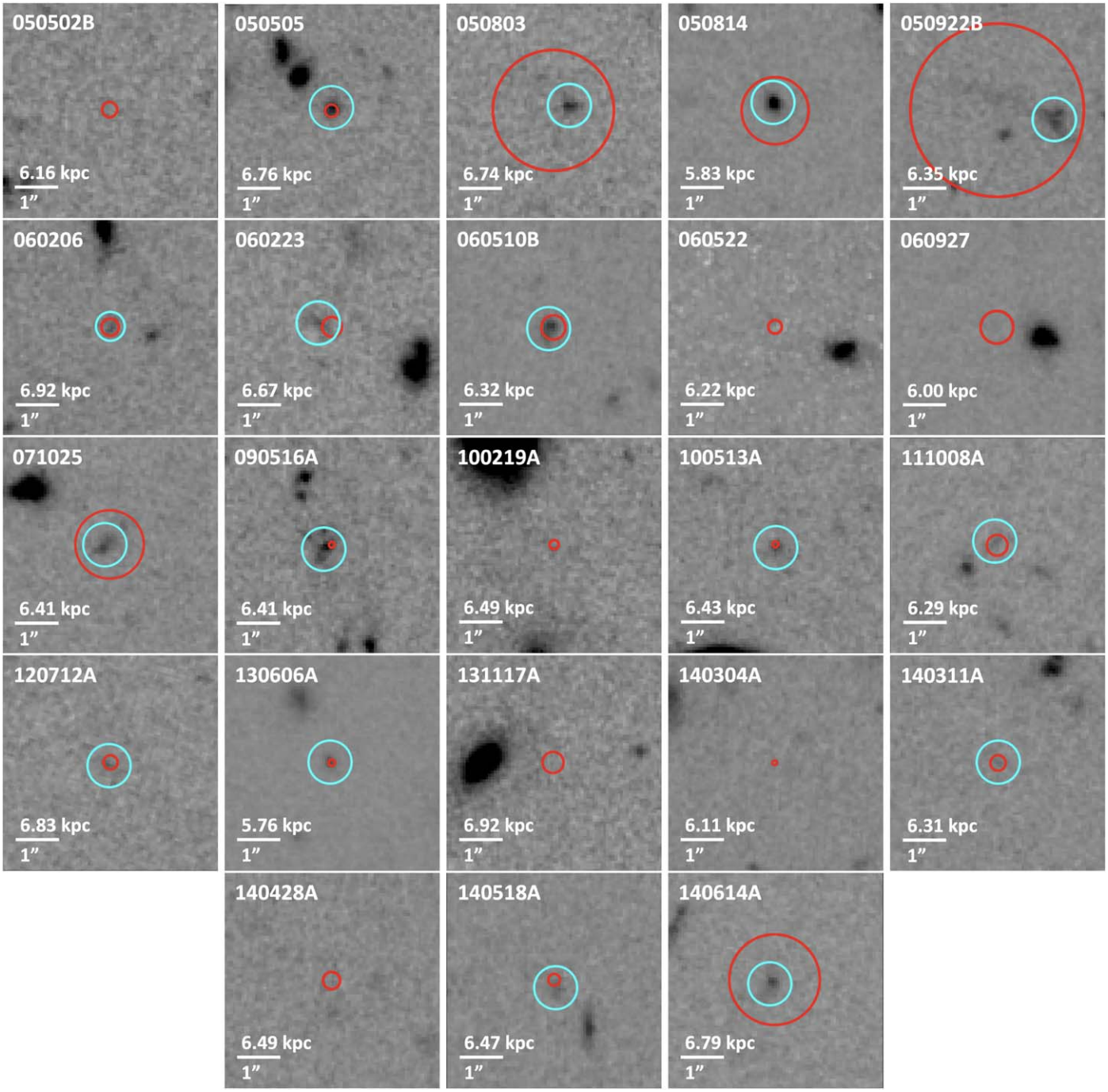

Figure 1. IR imaging from WFC3 of the 23 host galaxies. Each box is 5″ wide. The afterglow position is shown in red with either the 3σ radius or with the Swift-XRT radius, while the host (when detected) is identified by a cyan 0.″5 radius region. Positions of both the afterglow and host are reported in Tables 1 and 2, respectively. North is up and east is to the left.

Schlafly & Finkbeiner 2011) at the location of the afterglow. We assume a UV spectral slope of $\beta = -2$ (see Figure 2 in Wilkins et al. 2013), where $f_\nu \propto \nu^{-\beta}$ and then apply a K-correction of $-2.5\log_{10}(1+z)$. The component of the K-correction for the spectral shape is proportional to $(2+\beta)$, and therefore vanishes since we assume $\beta = -2$. In summary:

$$M_{1600\text{Å}} = m_{\text{F110W}} + 2.5\log_{10}(EE_{\text{frac}}) - A_{\text{MW}} + 5 \\ -5\log_{10}(D_L/pc) + 2.5\log_{10}(1+z),$$

where D_L is the luminosity distance. We report in Table 2 absolute magnitude, $M_{1600\text{Å}}$, uncertainties as the uncertainty on the apparent magnitude as reported by `Source Extractor` with propagation of the redshift uncertainty, when reported.

We report 3σ lower limits on the observed magnitude for sources that are not detected in our images. In each HST image of a nondetected galaxy, we measure the flux within randomly placed 0.″37 radius apertures within 6″ of position of the afterglow. This aperture size was chosen as it is the average

Table 2
Photometry of the Host Galaxy Detections

GRB	R.A. (J2000)	Decl. (J2000)	m_{F110W} (mag AB)	A_{MW} (A_{F110W})	M_{UV} (mag AB)
050505	09:27:03.2886	+30:16:23.988	25.95(0.10)	0.031	−20.42(0.10)
050803	23:22:37.8142	+05:47:08.511	26.08(0.11)	0.067	$-20.33(^{+1.51}_{-0.39})$
050814	17:36:45.3861	+46:20:21.756	25.46(0.03)	0.069	−21.47(0.06)
050922B	00:23:13.2809	−05:36:17.513	25.37(0.08)	0.032	$-21.21(^{+0.34}_{-0.19})$
060206	13:31:43.4549	+35:03:03.208	27.56(0.22)	0.022	−18.67(0.22)
060223	03:40:49.5884	−17:07:48.258	26.63(0.07)	0.101	−19.96(0.07)
060510B	15:56:29.6623	+78:34:12.065	26.05(0.06)	0.020	−20.58(0.06)
071025	23:40:17.0939	+31:46:42.862	26.06(0.10)	0.065	−20.51(0.25)
090516A	09:13:02.6094	−11:51:15.152	25.04(0.07)	0.044	−21.24(0.07)
100513A	11:18:26.8473	+03:37:39.837	26.65(0.15)	0.048	−19.89(0.15)
111008A	04:01:48.2556	−32:42:33.164	27.69(0.30)	0.005	−18.87(0.30)
120712A	11:18:21.2274	−20:02:01.369	27.06(0.12)	0.037	−19.26(0.12)
130606A	16:37:35.1338	+29:47:46.549	26.79(0.05)	0.015[a]	−20.26(0.05)
140311A	13:57:13.2765	+00:38:31.414	28.38(0.35)	0.033	−18.18(0.35)
140518A	15:09:00.5975	+42:25:05.708	27.22(0.13)	0.040	−19.31(0.13)
140614A	15:24:40.5339	−79:07:43.346	26.14(0.09)	0.109	−20.28(0.09)

Notes. From left to right: name of the GRB, host centroid position in ICRS, apparent magnitude of the host galaxy as reported from `Source Extractor`, Galactic extinction from NED (Schlafly & Finkbeiner 2011), and the absolute UV magnitude of the host galaxy as converted using the methods described in Section 2. The uncertainty on the absolute magnitude also accounts for that in redshift.
[a] Galactic extinction for GRB 130606A is A_{F140W}.

radius used for the detections. We calculate the median flux within these regions, and we clip any flux measurements with a $>3\sigma$ divergence from this value and then recalculate the median. We repeat this 3σ median-clipping procedure until convergence of the median. Three standard deviations above this median value is used as an upper limit for the magnitude of the host galaxy. We then aperture correct these limits using the same methods as were used for the detections and report these final upper limits in Table 3. These galaxy magnitudes, both detections and upper limits, were derived in this way for modeling and comparison of the UV LF of our sample, which we detail in Section 3.

Table 3
Photometry for the Host Galaxy Nondetections.

GRB	m_{F110W} (mag AB)	A_{MW} (A_{F110W})	M_{UV} (mag AB)
050502B	>27.55	0.026	>−19.10
060522	>27.83	0.048	>−18.67
060927	>27.84	0.054	>−18.76
100219A	>27.58	0.067	>−18.78
131117A	>27.39	0.016	>−18.67
140304A	>27.49	0.049	>−19.05
140428A	>27.66	0.019	>−18.95

Note. From left to right, apparent magnitudes (as 3σ above sky and EE corrected), Galactic extinction from NED (Schlafly & Finkbeiner 2011), and extinction-corrected absolute magnitudes as converted using the methods described in Section 2. When applicable, the redshift uncertainty was propagated, and the brighter limit was chosen.

3. Discussion

3.1. Lyman-break Galaxy Ultraviolet Luminosity Functions

We derive the luminosity distribution of our GRB host galaxy sample from Tables 2 and 3. We compare these results to samples of Lyman-break galaxies at $z\sim5$ from Bouwens et al. (2021; hereafter B21a) and Finkelstein et al. (2015; hereafter F15). These LFs are based on the largest and most complete samples of these galaxies in the relevant redshift range. As such, they provide a good representation of the state of knowledge of the Lyman-break galaxy LF at $z\sim5$ and provide some indication of systematic variations that may be due to the different approaches of the these independent teams. We elected to not use results from the more recent Bouwens et al. (2022a) due to their choice of functional form for the LF, which deviates from the standard Schechter function by including an additional parameter, δ, that allows for curvature at the faint end ($M_{UV}>-16$ mag) of the LF. Their formula and best-fit parameters result in a divergent LF whose CDF is inherently highly sensitive to the choice of the lower integration limit. Furthermore, since our faintest detected GRB host galaxy is at $M_{UV}=-18.1$ mag and even the upper limits for our nondetections are not much fainter than this, our data are insensitive to the shape of the faint-end LF and could not place any meaningful limitations on this additional parameter. Indeed, even with their larger sample of 59 $z\sim5$ Lyman-break galaxies, they find $\delta=0.07\pm0.2$, to an uncertainty $5\times$ greater than that they find for their α (0.04). The Schechter function parameters from both B21a and F15 are reported in Table 4.

To compare the Lyman-break galaxy LFs of B21a and F15 meaningfully to that of our GRB host galaxies (detailed in the following sections), we must first account for the GRB-production rate. To do so, it is necessary to weight the Lyman-break galaxy LFs by the instantaneous SFR, as the GRB-production rate is expected to be proportional to the SFR. The SFR is proportional to the intrinsic UV luminosity (Kennicutt 1998), and so we can effectively account for GRB selection effects by multiplying the Lyman-break galaxy LF by the intrinsic luminosity of the Lyman-break galaxy. We consider two conversions of the intrinsic to the observed UV luminosity, as the LFs are functions of the observed luminosity. In both cases, we construct the base SFR-weighted Schechter

Table 4
Best-fit Schechter Function Fit Parameters to the GRB Host Data and the Lyman-break Galaxy Data Sets

Formalism	α	M_* (mag)
Linear L-conversion	$-1.30^{+0.30}_{-0.25}$	$-20.33^{+0.44}_{-0.54}$
O11 formalism	$-1.47^{+0.30}_{-0.25}$	$-20.25^{+0.43}_{-0.51}$
Meurer et al. (1999; hereafter M99) formalism	$-1.49^{+0.30}_{-0.25}$	$-20.25^{+0.42}_{-0.51}$
Lyman-break Galaxy Samples		
B21a	$-1.74^{+0.06}_{-0.06}$	$-21.10^{+0.11}_{-0.11}$
F15	$-1.67^{+0.05}_{-0.06}$	$-20.81^{+0.12}_{-0.12}$
van der Burg et al. (2010)	$-1.65^{+0.09}_{-0.08}$	$-20.94^{+0.10}_{-0.11}$
Ono et al. (2018)	$-1.60^{+0.06}_{-0.05}$	$-20.96^{+0.06}_{-0.05}$
Harikane et al. (2022)	$-1.76^{+0.04}_{-0.03}$	$-21.09^{+0.04}_{-0.03}$

Note. The fits to the GRB hosts were measured from our `RStan` program, while fits to the Lyman-break galaxies were copied from the listed citations.

LF (i.e., a predicted GRB host LF) as below:

$$\phi(L_{\rm obs}) = \left(\frac{\phi_*}{L_*}\right)\left(\frac{L_{\rm obs}}{L_*}\right)^{\alpha} e^{-L_{\rm obs}/L_*} \times L_{\rm int} \quad (1)$$

where L_* is the characteristic luminosity, $L_{\rm int}$ is the intrinsic luminosity, $L_{\rm obs}$ is the observed luminosity, ϕ_* is a normalization parameter, and α is the faint-end slope, as is standard in the Schechter function. In magnitude space, this can be restated as:

$$\phi(M_{\rm obs}) = \phi_{**}(10^{f(M_{\rm obs})})^{(\alpha+1)} e^{-10^{f(M_{\rm obs})}} \times 10^{-0.4\times M_{\rm int}} \quad (2)$$

where $f(M_{\rm obs}) = 0.4 \times (M_* - M_{\rm obs})$, $M_{\rm int}$ is the intrinsic magnitude, $M_{\rm obs}$ is the observed magnitude, ϕ_{**} is a normalization parameter, and α is still the faint-end slope. M_* is the characteristic magnitude and is defined as $M_* = -2.5 \times \log \frac{L_*}{L_0}$, where L_0 is the luminosity of a source with an absolute magnitude of 0.

1. In our first formalism, we assume a luminosity-independent dust contribution where the intrinsic luminosity, $L_{\rm int}$, is linearly proportional to the observed luminosity, $L_{\rm obs}$. Here, $L_{\rm int} \propto L_{\rm obs} \propto 10^{-0.4\times M_{\rm obs}}$.
2. Our second formalism is one where we assume a nonlinear luminosity-dependent dust contribution. We make this assumption because we expect more massive galaxies to have more dust. We construct this formalism from the following two relations from O11[13] and Bouwens et al. (2014), respectively:

$$A_{1600} = 1.81\beta + 4.01, \quad (3)$$

where A_{1600} is the extinction at 1600 Å and β is defined as:

$$\beta = -1.91 - 0.14(M_{\rm UV} + 19.5). \quad (4)$$

Since A_{1600} cannot be negative, this results in a piecewise LF of the form of Equation (1) where now

$$L_{\rm int} \propto 10^{-0.4\times M_{\rm obs}} \text{ for } M_{\rm obs} > -17.3 \quad (5)$$

and

$$L_{\rm int} \propto 10^{-0.4\times(1.25\times M_{\rm obs}+4.39)} \text{ for } M_{\rm obs} \leqslant 17.3 \quad (6)$$

3. Our third formalism is one where we again assume a nonlinear luminosity-dependent dust contribution, however we substitute for Equation (3) an estimation of the same relation from M99:

$$A_{1600} = 1.99\beta + 4.43 \quad (7)$$

We refer to our second and third formalisms as "O11" and "M99," respectively, in reference to the choice of the $A_{1600}(\beta)$ formulation (i.e., the choice of Equations (3) or (7)).

3.2. Gamma-Ray Burst Host Ultraviolet Luminosity Function

We use Bayesian hierarchical modeling to constrain the parameters of the luminosity distribution of the GRB host galaxies. We assume the galaxies follow a SFR-weighted Schechter function (see Equation (1)) with a faint-end magnitude limit of $M_{\rm UV} = -14.1$ mag (this arbitrary magnitude choice converts to a convenient value in our luminosity units and is well below our detection threshold in all cases, although we find that our results are not statistically sensitive to this precise choice). We used weakly informative Gaussian priors of $\mu_\alpha = -1.6$, $\sigma_\alpha = 1.0$ and $\mu_{\log L_*} = 10$, $\sigma_{\log L_*} = 1$ for the α and $\log L_*$ parameters, respectively. The model self-consistently included both the detections and the seven upper limits: the luminosity for each of these 23 objects was a free parameter in the model, and hence each has a corresponding posterior distribution. We symmetrized the uncertainties for each measurement, conservatively selecting the greater of the two, though we find that our results are also not sensitive to this choice. Four chains were run per model with at least 100,000 samples per chain after warm-up, which ensured negligible MCMC standard errors for all parameters of interest. In the final model runs, there were no divergences, and the chains for all parameters mixed well, with the convergence diagnostic $\widehat{R} = 1$. We complete this process three times, once each for our different considerations of the SFR-weight on the Lyman-break galaxy LF as described in the previous section. To model these luminosity distributions of the GRB host galaxies, we use the `Stan` software as implemented in version 2.26.13 of the `RStan` package (Stan Development Team 2024).

We show the posteriors and best-fit SFR-weighted Schechter functions for the L-independent and O11 weightings in Figure 2. These best-fit α and M_* parameters, along with their 1σ uncertainties, are provided in Table 4 as well as the same parameters for the M99 weighting. The Schechter parameters from B21a ($\alpha = -1.74 \pm 0.06$ and $M_* = -21.10 \pm 0.11$ mag) are consistent to within 2σ to our O11 best-fit parameters ($\alpha = -1.47 \pm 0.27$ and $M_* = -20.25 \pm 0.47$ mag). The same is true for the parameters from F15 as well as for those from other $z \sim 5$ Lyman-break galaxy LF studies (e.g., van der Burg et al. 2010; Ono et al. 2018; Harikane et al. 2022). These Lyman-break galaxy fits are consistent to within 2σ to our L-independent weighting as well. The slightly better agreement of the Lyman-break galaxy LFs to the O11 formalism is expected, as this formalism offers a more realistic estimate of the intrinsic extinction at $z \sim 5$. Along this parametric comparison, there is

[13] The amount of host UV extinction due to dust at $z \sim 5$ is an active area of research. The choice for this correction has often been that from M99, $A_{1600} = 4.43 + 1.99\beta$. However, there have been several updates to this relation (e.g., O11; Takeuchi et al. 2012; Bouwens et al. 2014; Casey et al. 2014). Here, we elect to use the relation from O11 (as stated in Equation (3)), as it is measured from Lyman-break analog galaxies, which offers the closest comparison to our GRB hosts.

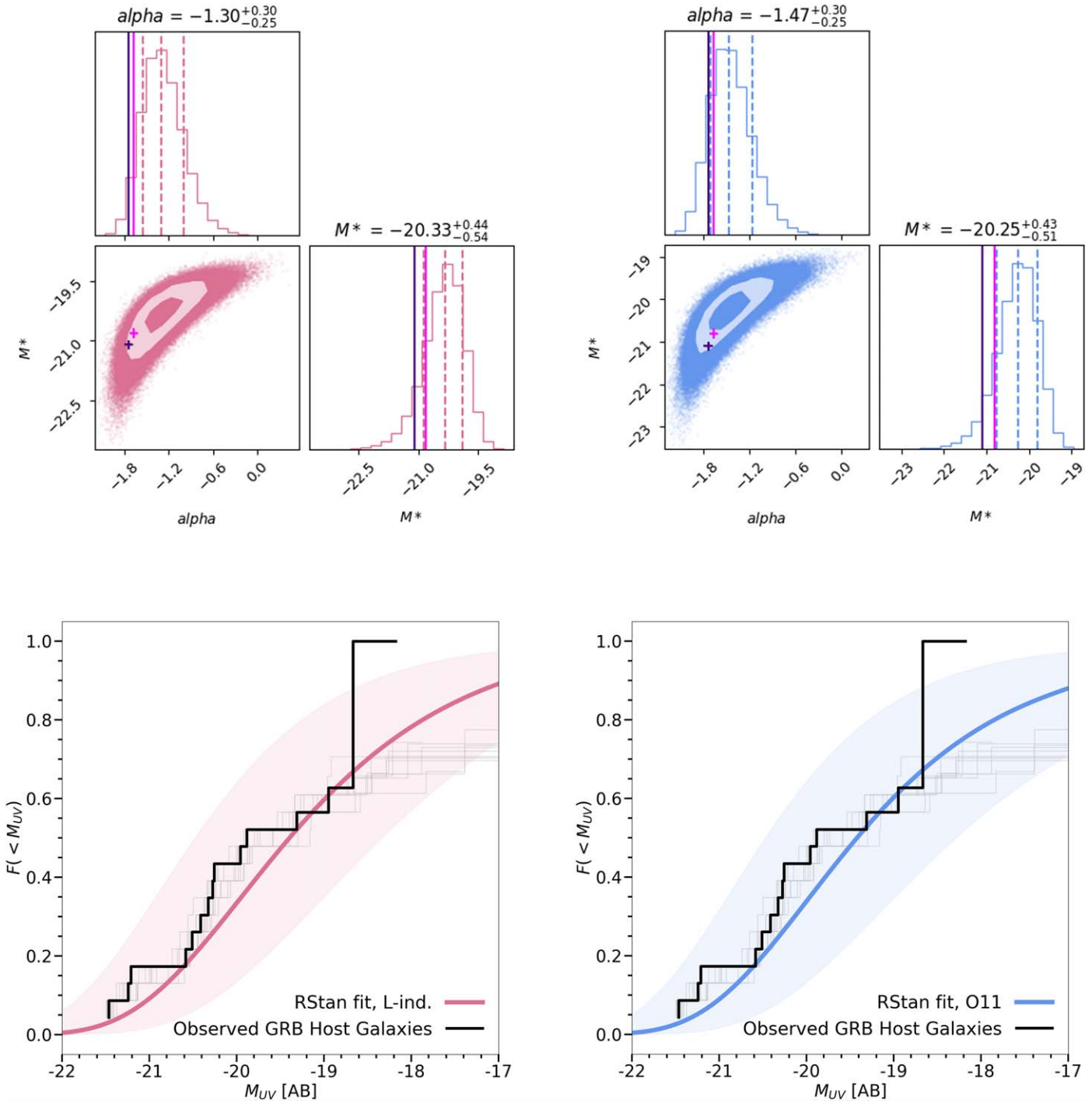

Figure 2. Top: correlations and marginalized posterior densities for α and M_* in the star formation rate (SFR)-weighted UV LF for the L-independent (pink) and Overzier et al. (2011; hereafter O11; blue) extinction corrections. The indigo lines show the α and M_* parameters from Bouwens et al. (2021), while the fuchsia lines show the same parameters for Finkelstein et al. (2015). These parameters are also shown with their uncertainty as crosses in the center panels. 1σ and 2σ contours are shown in the 2D histograms. Bottom: the observed cumulative distribution functions (CDFs) of and best fits to the UV LF for GRB host galaxies at $z \sim 5$. As indicated in the legend, the model shown in pink assumes an L-independent extinction correction and the model in blue assumes the O11 extinction correction. The black line is the observed GRB host galaxy CDF. The same 10 random draws from the modeled data are shown in silver.

no evidence of disagreement between the GRB host galaxy sample and the Lyman-break galaxy samples.

While the differences between the galaxy samples are not statistically significant, the best fits to the GRB host galaxies have a shallower α and a fainter M_*. With a larger GRB host galaxy sample, if these parameter differences were to become statistically significant, the move toward a shallower α and a fainter M_* would indicate that Lyman-break galaxy LFs overpredict the amount of faint star formation.

We construct a CDF of the GRB host galaxy LF by using Kaplan–Meier estimation (Kaplan & Meier 1958) on our observed magnitudes and upper limits. We plot this CDF in Figures 2 and 3. We qualify the uncertainty on this CDF by plotting also a subset of the CDFs created from random draws

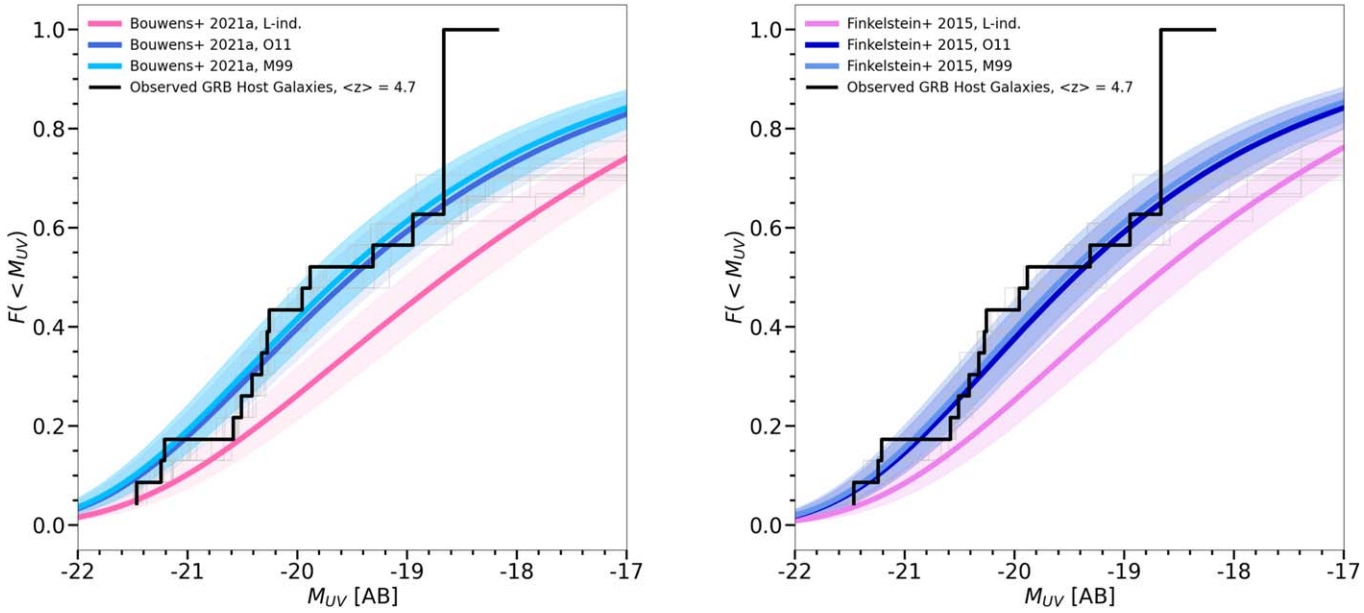

Figure 3. Left: observed CDF of the UV LF for GRB host galaxies at $z \sim 5$ [black] compared to the $z \sim 5$ CDFs of the SFR-weighted Lyman-break galaxies from B21a with the luminosity-independent galaxy extinction correction in pink and with the empirical luminosity-dependent galaxy extinction from Bouwens et al. (2015) and O11 in dark blue and the empirical luminosity-dependent galaxy extinction from Bouwens et al. (2015) and M99 in light blue. Uncertainties in the Lyman-break galaxy relations are shown as shaded regions and represent the 1σ uncertainties of the LF parameters [light pink and light blues]. Uncertainty in the GRB host galaxy LF is shown with 10 random pulls of the modeled GRB host galaxy magnitudes [silver]. Right: a similar plot to that on the left, with the same GRB host galaxy LF, but using as comparison now the $z \sim 5$ SFR-weighted UV LF from F15. The pink LF again contains the assumption that galaxy extinction is luminosity independent, while the LF in dark blue (light blue) assumes the O11 (M99) extinction correction.

of the modeled magnitude sets. In this figure we also show the CDFs of the UV LFs from B21a and F15 with the different extinction assumptions.

To measure the likelihood of inconsistency between the Lyman-break galaxy and metallicity-biased GRB host galaxy luminosity distributions to that of the observed $z \sim 5$ GRB host galaxy distribution, we use a log-rank test. This test was chosen because for its applicability to distributions including censored data (i.e., our upper limits), unlike commonly used statistical tests, like a Kolmogorov–Smirnov (Massey 1951) or an Anderson–Darling test (Stephens 1974). We report the p-value corresponding to the calculated χ^2 statistic for each test in Table 5. This p-value is the probability of achieving the χ^2 test statistic, and so since we consider a 2σ threshold, we accept $p < 0.05$ as confirmation for the null hypothesis that the compared samples are pulled from different distributions. To complete these tests, we use `survdiff` within the `survival` package in R (Terry & Patricia 2000; R Core Team 2023; Therneau 2024).

With p-values all above $p = 0.05$, we find no evidence for inconsistency between our O11 and M99 SFR-weighted Lyman-break galaxy luminosity distributions and our derived GRB host galaxy luminosity distribution. We do, however, find 2σ disagreement (though 3σ agreement) between our L-independent SFR weighting for both the B21a and F15 Lyman-break galaxy luminosity distributions and that of our GRB host galaxies. These results imply that if GRBs are to trace star formation, either the L-independent extinction correction is an incorrect assumption for the distribution of dust in $z \sim 5$ star-forming galaxies or additional parameters are necessary, perhaps the faint-end slope curvature parameter δ presented in Bouwens et al. (2022a).

Table 5
Results of the Log-rank Tests between the $z \sim 5$ GRB Host Galaxy Luminosity Function Derived in This Paper and the SFR-weighted Lyman-break Galaxy Luminosity Functions and the Predicted Metallicity-biased GRB Host Galaxy Luminosity Functions

Comparison	log-rank p-value
B21a linear	0.011
B21a O11	0.273
B21a M99	0.368
F15 linear	0.007
F15 O11	0.167
F15 M99	0.228
T15 $p = 0$	2.33×10^{-7}
T15 $p = 0.04$	3.71×10^{-5}
T15 $p = 0.2$	0.002
T15 $p = 1000$	0.108

Note. The SFR-weighted Lyman-break galaxy LFs are listed by the different SFR weights. The $z = 4.75$ metallicity-biased LFs are listed by the plateau parameter, as described in Section 3.3.

3.3. Investigating the Metallicity Bias

Lastly, we consider the influence of metallicity in our LF fits. To quantify GRB-production metallicity sensitivity, we consider the UV LF predictions at $z = 4.75$ from T15). Those authors developed a model that considers two GRB progenitor pathways: one that is metallicity dependent and one that is metallicity independent, which they refer to as "metallicity sensitive" (MS) and "metallicity insensitive" (MI) channels. They quantify the percentage of GRBs originating from a MI pathway with their "GRB efficiency" function, $\kappa(Z)$. This is

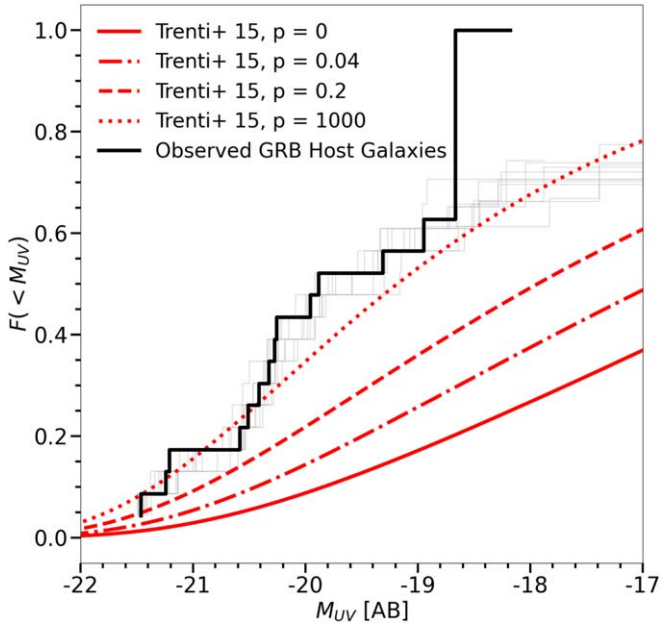

Figure 4. Our $z \sim 5$ GRB host galaxy LF as described in Figure 3 and predicted GRB host LFs at $z = 4.75$ from Trenti et al. (2015). Described in detail in Section 3.3, the p-parameter is tied to the influence of metallicity on the GRB progenitor path. Across all redshifts, when $p = 0$, there is a metallicity bias where GRBs cannot be produced in environments with $Z > Z_{\odot}$, and when p tends to infinity, GRB creation is MI. In Trenti et al. (2015), they report Schechter function LF parameters for four choices of p, which we plot here. The results from log-rank tests between the black, median LF for our GRB host sample, and the four metallicity-biased LFs are shown in Table 5.

defined as:

$$\kappa(Z) = \kappa_0 \times \frac{a \log_{10} Z/Z_{\odot} + b + p}{1 + p},$$

where κ_0, a, and b are piecewise defined based on galaxy metallicity and take on the same values as in T15. In this context, p is what they refer to as the "plateau" parameter and can take on any nonnegative value.

In the low-metallicity (and therefore high-z) limit, this MI efficiency function, $\kappa(Z)$, asymptotically "plateaus" to the value $p/(1+p)$. While p is explicitly *not* a probability (and can take on any nonnegative value), it is correlated with the percentage of GRBs originating from the MI channel. Across all metallicities and redshifts, when $p = 0$, it is assumed that GRBs originate exclusively from the MS channel, and when $p = \infty$, it is assumed GRBs originate exclusively from the MI channel. Positive and finite values of p assume a split of GRB progenitor paths. Trenti et al. (2015) applied their models to the Swift GRB catalog and to other GRB host galaxy samples (Savaglio et al. 2009; Cucchiara et al. 2015) and found that $p = 0.2$ best replicates the redshift evolution of the GRB rate to $z \sim 6$. At $z \sim 5$, the majority of galaxies have metallicities below the threshold values found in the local Universe, so we expect the host galaxy LF to be more consistent with the MI parameterization, $p = \infty$.

We show in Figure 4 the four $z = 4.75$ LFs predicted by Trenti et al. (2015) for different values of p overlaid on our GRB host galaxy LF, and we report the results of log-rank tests between these relations in Table 5. We find only the $p = 1000$ case to be consistent with our LF to within the Gaussian-equivalent 2σ. Specifically, we find disagreement with our observations and the $p = 0.2$ model favored by Trenti et al. (2015). The disagreement of the $p = 0.2$ model with the high-redshift host galaxy LFs (ours at $z \sim 5$ and that at $z \sim 3.5$ from Greiner et al. 2015) implies that a different metallicity parameterization for GRB production is necessary.

Table 6
Host Galaxy Size

GRB	$R_{\rm eff}$ (pixel)	$R_{\rm eff}$ (pc)
050505	1.14(0.24)	501 ± 105
050803	2.87(0.20)	1258^{+271}_{-119}
050814	1.00(0.11)	379 ± 42
050922B	4.47(0.21)	1844^{+135}_{-103}
060206	1.78(1.04)	800 ± 467
060223	1.67(0.18)	724 ± 78
060510B	2.85(0.07)	1171 ± 29
071025	3.28(0.24)	1366^{+113}_{-114}
090516A	5.72(0.22)	2556 ± 98
100513A	1.28(0.21)	535 ± 88
111008A	<2.30	<940
120712A	1.47(0.26)	652 ± 115
130606A	2.64(0.13)	988 ± 49
140311A	<1.90	<778
140518A	1.58(0.27)	664 ± 114
140614A	4.03(0.21)	1778 ± 93

Note. From left to right the columns are the name of the GRB, the half-light radius ($R_{\rm eff}$) in pixels, and $R_{\rm eff}$ in parsecs. When applicable, the redshift uncertainty was propagated.

3.4. Gamma-Ray Burst Host Size Distribution

Observations of Lyman-break galaxies have shown a correlation between UV luminosity and half-light radius (Kawamata et al. 2015; Shibuya et al. 2015; Bouwens et al. 2022b). Studies of the sizes of GRB host galaxies have shown that they are, on average, smaller than the general population at $z < 1$ but by $z \sim 3$ they have comparable sizes (Conselice et al. 2005; Kelly et al. 2014; Lyman et al. 2017; Schneider et al. 2022). Additionally, Wainwright et al. (2007) showed evidence for a size–luminosity relation for GRB host galaxies at $0 < z < 3$, with $\langle z \rangle \sim 1$. We investigate this relation and how it compares to that of field galaxies of our sample of GRB host galaxies at $z \sim 5$. We present half-light radii ($R_{\rm eff}$) for our 16 detected host galaxies in Table 6 and Figure 5. We first constructed point-spread functions (PSFs) for each of our two filters, F110W and F140W. Schneider et al. (2022) found that for a sample of the fields of 42 GRB host galaxies at $z \sim 2$ imaged with WFC3/F160W, the constructed PSF had a radius profile stable against the choice of field in which to select stars for the star catalog but had a signal-to-noise ratio that was dependent on the number of stars selected, increasing with the size of the star catalog. In their study of GRB host half-light radii at $z \sim 2$, Schneider et al. (2022) find that $N \sim 30$ is a sufficient size for the catalog. We apply this finding to our sample and use 33 stars from the fields of GRBs 050814 and 050922B to construct the PSF for F110W. The choice of these fields was mostly arbitrary, however we chose not to use fields crowded with several saturated stars (such as that of GRB 140614A). We had only one GRB field imaged in F140W, and so we select 26 stars from the field of GRB 130606A to construct the PSF for this filter. We use the `astropy` package `EPSFBuilder` (Bradley et al. 2023) to generate the two PSFs from these star catalogs.

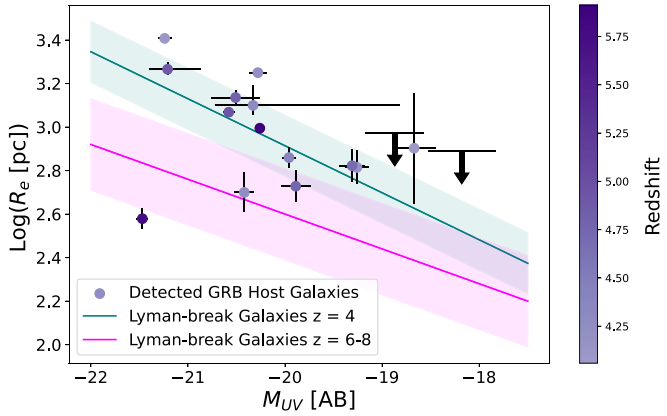

Figure 5. Galaxy size vs. absolute UV magnitude relation for Lyman-break and GRB host galaxies. GRB host measurements and their uncertainties are shown as shaded purple points and black crosses and are published in Tables 2 and 6. The points are shaded by their redshift as indicated in the color bar to the right. The outlier point on the bottom left is that of the host galaxy of GRB 050814. The relations for Lyman-break galaxies at $z = 6$–8 [magenta] and at $z = 4$ [teal] are from Bouwens et al. (2022b). The shaded regions show the the 1σ scatter of each relation.

We measure the half-light radii of our detected GRB host galaxies by fitting a Sérsic light profile with GALFIT (Peng et al. 2010). On our first measurement attempt, we use as guesses the results from Source Extractor with GALFIT able to fit all parameters. If the program was not able to converge all parameters, we try again holding $R_{\rm eff}$ constant but all other parameters open. If the other parameters converge on this run, we fix the parameters to these new values and allow for GALFIT to fit for $R_{\rm eff}$ on the next run. If the parameters do not converge, or if $R_{\rm eff}$ does not converge as the only free parameter, we instead try fixing all parameters to the Source Extractor guesses and allowing the program to fit for only $R_{\rm eff}$. If there still was no convergence, and there was a second source within 20 pixels of the host, we rerun the program with a second Sérsic profile for the second source. We use the same methods to attempt convergence for both sources. In all cases, if there was sufficient convergence, the residual was visually checked for confirmation of a good fit. We record $R_{\rm eff}$ and its uncertainty reported by GALFIT in Table 6.

For three of our sources (the host galaxies of GRBs 050814, 111008A, and 140311A), no runs were successful following this procedure, meaning either no convergence of $R_{\rm eff}$ or a visually bad residual. For the host galaxies of GRBs 111008A and 140311A, we adopt $R_{\rm eff}$ upper limits as those reported by Source Extractor. For the host galaxy of GRB 050814, we updated the Source Extractor guesses to our best guesses, with our only change being updating the position angle (PA) from $-61°$ to 40°. With this update, GALFIT converged all parameters. This fit is elaborated upon in the Appendix entry for GRB 050814.

We compare this sample of GRB host galaxy sizes to Lyman-break galaxy sizes at $z \sim 4$ and $z \sim 6$–8 (Bouwens et al. 2022b) in the form of a size–luminosity relation in Figure 5. Under the assumption that GRBs unbiasedly trace star formation, we expect $z \sim 5$ GRB host galaxies to fall in between the $z \sim 4$ and $z \sim 7$ relations. Since our smaller sample has an average $z = 4.6$, if this assumption is to be true, we would expect the GRB host sample to be weighted closer to the $z \sim 4$ relation. We find that ∼68% (11/16) of our GRB host galaxies fall within or below the 1σ scatter of the $z \sim 4$ relation. This supports our claim that at $z \sim 5$, Lyman-break and GRB host galaxies trace the same stellar populations.

3.5. Gamma-Ray Burst Host Galaxy Nondetection Fraction and Implications of Hidden Star Formation

The source of the UV photons needed to reionize the intergalactic medium in the early Universe has been and continues to be an area of very active research (Furlanetto & Mesinger 2009; Robertson et al. 2015; Endsley et al. 2023). One explanation for this process is the UV radiation from massive stars in star-forming galaxies (Madau et al. 1999; Ciardi et al. 2000; Bunker et al. 2004, 2010; Finkelstein et al. 2010, 2012). Until recently, with the launch of JWST, investigations of the feasibility of this explanation have mostly stopped at $z \sim 8$ or have relied on the extrapolation of the characterizations of lower-redshift observations of Lyman-break galaxies to higher redshifts and fainter magnitudes (Oesch et al. 2010; Bouwens et al. 2012). Recent JWST-based studies have found discrepancies from lower-z expectations and models, namely the detection of more massive, bright galaxies than expected (Harikane et al. 2023; Finkelstein et al. 2023). There have been many offered explanations for these discrepancies, including stochastic star formation (Furlanetto & Mirocha 2022; Mirocha & Furlanetto 2023; Shen et al. 2023) and high-efficiency star formation (Dekel et al. 2023).

While using GRBs to test the feasibility of massive star reionization of the Universe is not new (e.g., Tanvir et al. 2019), our complete GRB sample offers the first opportunity to test this feasibility with statistical robustness at a redshift just outside the "Epoch of Reionization." From our nondetection fraction, we can estimate the percentage of star formation that is occurring in galaxies fainter than our detection limit (i.e., galaxies that are intrinsically faint and galaxies that would otherwise be detected but are dust obscured). These are galaxies that are inherently often missed in star-forming galaxy samples as they are not directly observable. Comparing the direct measurement of the percentage of faint star formation to expectations from Lyman-break galaxy LFs is critical, as faint star-forming galaxies are thought to be important contributors of ionizing photons (McLure et al. 2010).

Under the assumption that GRBs unbiasedly trace star formation at this redshift, using binomial statistics, our nondetection fraction of 7/23 is consistent at the 95% confidence level with 13%–53% of star formation occurring in galaxies fainter than our detection limit of $M_{\rm UV} \approx -18.3$ mag. This measurement is unique in that it is independent of the functional form of the LF and offers a nonparametric way to test the consistency of an assumed functional form to an observed quantity. It is shown in Figure 3, that the percentage of undetectable star formation predicted by the SFR-weighted Schechter function Lyman-break galaxy LFs is $\sim 40\% \pm 5\%$ and $\sim 25\% \pm 5\%$ when considering L-independent and L-dependent (O11 and M99) host extinction, respectively. The lack of disagreement between all of the Lyman-break galaxy predictions and the GRB host galaxy measurement offers support for the hypothesis that star-forming galaxies are large contributors of ionizing photons in the early Universe.

4. Conclusions

We present new rest-frame UV HST imaging of a complete sample of 23 long-GRB host galaxies at $z \sim 5$. From our

imaging, we measure UV magnitudes and galaxy sizes. We detect 16 GRB host galaxies and place upper limits on the magnitudes of the remaining seven. Of the 16 detections, we are able to spatially resolve 14 and place upper limits on the sizes of the remaining two. Through the construction of a UV LF, we find that our GRB host sample is statistically consistent (log-rank test $p > 0.05$) with that of the star-forming galaxy population at the same redshift, when using reasonable corrections for the intrinsic extinction in star-forming galaxies. When investigating the feasibility of the metallicity-bias model of GRBs from Trenti et al. (2015), we find that our host sample is inconsistent with this model. Assuming a SFR-weighted Schechter function formalism and a GRB rate proportional to the dust-corrected UV luminosity, we find parametric agreement between both α and M_* of our best fits and those from B21a and F15, again regardless of our choice of galaxy extinction. We find that 11 of our 16 ($\sim$68%) host galaxies fall within or below the 1σ scatter of the size–luminosity relation of $z \sim 4$ star-forming galaxies from Bouwens et al. (2014). The lack of disagreement between the luminosity-dependent UV LFs and the size–luminosity relations between the Lyman-break and GRB host galaxy samples implies that at $z \sim 5$, GRBs are unbiased tracers of star formation.

Under this well-supported assumption that GRBs are unbiased tracers of star formation at this redshift, we use our nondetection fraction of $7/23$ and binomial statistics to estimate that, at 95% confidence, 13%–53% of star formation is undetected in observations of these depths. In other words, we find that up to $\sim$50% (or alternatively, only $\sim$10%) of star formation could be occurring in galaxies with $M_{\rm UV} > -18.3$ mag. This measurement is complementary to and unique from similar measurements from Lyman-break galaxy surveys since it is insensitive to the parameterization of the LF. This solidifies the importance of GRB afterglow and host galaxy observations as a tool for studies of high-z star formation.

The sample presented here is the largest and most complete sample of GRB host galaxies at this redshift. It is unlikely that this sample will be surpassed in statistical sensitivity in the near future, due to our bias-minimizing selection cuts. One of the selection criteria was a detection cut pre-2015. Since then, there have been 12 additional Swift-detected GRBs with $z > 4$. If all of these sources were to meet our sample criteria and followed our detection distribution, the addition of these 12 sources would improve our sensitivity by $\sim$40% (i.e., our uncertainty on the Schechter parameters would be reduced by $\sim$40%). While an improvement, this precision is still not better than that from Lyman-break galaxy samples and therefore the inclusion would not result in a significant statistical advance from the analysis performed here. What is needed to improve this analysis is, simply, the detection and follow up of many more high-redshift GRBs. There are missions, like the Space-based multiband astronomical Variable Objects Monitor (SVOM; Wei et al. 2016), Gamow Explorer (White et al. 2021), and The Transient High-Energy Sky and Early Universe Surveyor (THESEUS; Tanvir et al. 2021) planned expressly for such follow up. The analysis presented here shows directly how results from such missions can be interdisciplinary, improving not GRB science but our understanding of star-forming galaxies as well.

Acknowledgments

We thank Paolo D'Avanzo for assistance in accessing afterglow images at TNG, Wen-fai Fong for assistance in the $P_{\rm cc}$ calculations, and Kerry Paterson for assistance in afterglow alignment. We thank Daniel Brethauer, Lindsay DeMarchi, and Natalie LeBaron for their comments, which improved this manuscript. We thank the journal editor and anonymous referee for their suggestions, which helped to make the manuscript more clear.

The TRex team at UC Berkeley is supported in part by the National Science Foundation under grant No. AST-2221789 and AST-2224255, and by the Heising-Simons Foundation under grant no. 2021-3248. J.S. acknowledges support from the Packard Foundation. This research made use of Photutils, an Astropy package for detection and photometry of astronomical sources (Bradley et al. 2023). This work made use of data supplied by the UK Swift Science Data Centre at the University of Leicester. Support for program GO-15644 was provided by NASA through a grant from the Space Telescope Science Institute, which is operated by the Association of Universities for Research in Astronomy, Inc., under NASA contract NAS 526555. This research has made use of the NASA/IPAC Extragalactic Database (NED), which is funded by the National Aeronautics and Space Administration and operated by the California Institute of Technology. This research has made use of the Keck Observatory Archive (KOA), which is operated by the W. M. Keck Observatory and the NASA Exoplanet Science Institute (NExScI), under contract with the National Aeronautics and Space Administration. This research used the facilities of the Italian Center for Astronomical Archive (IA2) operated by INAF at the Astronomical Observatory of Trieste. Based on observations collected at the European Southern Observatory under ESO programs 077.D-0661(B), 083.A-0644 (B), 092.A-0124(A), and 093.A-0069(A).

Facilities: Gemini:Gillett (GMOS-N), Gemini:South (GMOS-S), HST (WFC3), Keck (LRIS), Palomar Observatory (P60), TNG (LRS), REM, Swift (XRT and UVOT), and VLT (FORS2, X-Shooter).

Software: `Astrodrizzle` (Gonzaga et al. 2012), Astropy (Astropy Collaboration et al. 2013, 2018, 2022), corner (Foreman-Mackey 2016), photutils (Bradley et al. 2023), `Source Extractor` (Bertin & Arnouts 1996), R (R Core Team 2023), RStan (Stan Development Team 2024), `survival` (Therneau 2024; Terry & Patricia 2000).

Appendix
Notes on Individual Gamma-Ray Burst Host Galaxies

The positions and uncertainties for all afterglows are reported in Table 1. The converted absolute magnitudes, Galactic dust corrections, and uncertainties for host galaxy detections are listed in Table 2. The converted absolute magnitudes and Galactic dust corrections for host galaxy nondetections are listed in Table 3. 5″ cutouts of the HST images centered on the position of the afterglow are presented in Figure 1.

A.1. GRB 050502B

GRB 050502B has a photometric redshift of $z = 5.2 \pm 0.3$ as measured from *R*- and *I*-band imaging from TNG of the afterglow (Afonso et al. 2011). We identify a source in the stacked *I*-band TNG image from 2005 May 3 within the 1.″5

Swift-XRT error circle. The centroid of the afterglow was measured to an uncertainty of 0.″041 using Source Extractor, and the astrometric alignment to the HST image had a measured rms uncertainty of 0.″043 using TweakReg. These uncertainties are added in quadrature for a total positional uncertainty on the afterglow of 0.″060. Within a 3σ (0.″18) radius region in the HST image at the position of the afterglow, there is no source detected with Source Extractor. We find two sources within a 5″ box centered at the position of the afterglow, and we calculate P_{cc} values for both above 0.6. For this reason we consider the host of this GRB to be a nondetection. Following the prescription in Section 2, we estimate a limiting magnitude of $m_{F110W} > 27.55$ mag at 3σ above background in a 0.″37 radius aperture.

A.2. GRB 050505

GRB 050505 has a spectroscopic redshift of $z = 4.275$ from Keck/LRIS afterglow spectroscopy analyzed in Cenko et al. (2005). With Keck/LRIS *I*-band imaging from 2005 May 6, we identify a source within the Swift-XRT error region. We estimate an uncertainty on the centroid of 0.″0024 and an uncertainty on the astrometric alignment to the HST image of 0.″050. These uncertainties are added in quadrature for a total afterglow positional uncertainty of 0.″050. The afterglow and its 3σ uncertainty region are coincident with a source in the HST image. We calculate $P_{cc} = 0.02$ for this source, and we identify it as the host of this GRB. We report a measured apparent magnitude of $m_{F110W} = 25.95 \pm 0.10$ mag.

A.3. GRB 050803

GRB 050803 has a photometric host galaxy redshift of $z = 4.3^{+0.60}_{-2.40}$ as detailed in Perley et al. (2016a). All optical afterglow imaging referenced in the General Coordinates Network (GCN) circulars for this source was for a misidentified source at $z = 0.4$, and consequently the afterglow position we report is the enhanced Swift-XRT position with its 1.″4 uncertainty. The MAST-assigned WCS for the WFC3/F110W image was incorrect by several arcseconds, however, we were able to correct this with alignment to a WFC3/F160W image (ID: 12307, PI: Levan) of the same field. This alignment has an uncertainty of 0.″094. Within the Swift-XRT region in the HST image, we detect only one source. This source is consistent with that reported in Perley et al. (2016a) used to identify the photometric host galaxy redshift, and we therefore classify it as the host galaxy of this GRB. Using Source Extractor, we measure an apparent magnitude of this host galaxy of $m_{F110W} = 26.08 \pm 0.11$ mag. We calculate $P_{cc} = 0.35$ for this source when using the 90% confidence Swift-XRT uncertainty as R_e. This percent chance coincidence is well above our 10% threshold. When estimating the impact of false host-association contamination in our sample, we also consider the possibility that this is a nondetection with a measured limiting magnitude of $m_{F110W} > 27.16$ mag.

A.4. GRB 050814

GRB 050814 has a photometric afterglow redshift of $z = 5.77$ as reported in Curran et al. (2008). We detect the afterglow in stacked P60 *i*-band imaging from 2005 August 15. We report an uncertainty on the centroid of the afterglow of 0.″16, and an uncertainty on the astrometric alignment to the HST image of 0.″20, for a total positional uncertainty of 0.″257. Within a 0.″78 radius region centered at the afterglow position in the HST image, we detect a single source for which we calculate $P_{cc} = 0.08$. We identify this source as the host galaxy of GRB 050814 and measure an apparent magnitude of this galaxy of $m_{F110W} = 25.46 \pm 0.03$ mag.

GALFIT was unable to converge on a single Sérsic profile, following our standard methods of using the Source Extractor parameter results as input. We were able to achieve converge after modifying the PA guess from −61° to 40°, our estimate of the PA of the galaxy. While all parameters converged and the residual image of this solution passed our visual check, the Sérsic index, *N*, converged to $N = 9.97 \pm 3.03$, which is much larger than expected. We also attempted to fit the galaxy with two Sérsic components and achieved convergence for both profiles, but the residual did not pass our visual check. We chose to complete the analysis with the R_{eff} from the single component solution, $R_{eff} = 1.00 \pm 0.11$ pixel.

A.5. GRB 050922B

GRB 050922B has no afterglow detections reported in the literature but has a photometric host redshift of $z = 4.9^{+0.3}_{-0.6}$ as detailed in Perley et al. (2016a) from *i*- and *z*-band Gran Telescopio CANARIAS (GTC)/OSIRIS imaging. We detect three sources within the Swift-XRT error circle including the source identified in Perley et al. (2016a). We measure an apparent magnitude of this source of $m_{F110W} = 25.37 \pm 0.08$ mag. We calculate $P_{cc} = 0.44$ for this source when using the 90% confidence Swift-XRT uncertainty as R_e. This percent chance coincidence is well above our 10% threshold. When estimating the impact of false host-association contamination in our sample, we also consider the possibility that this is a nondetection with a measured limiting magnitude of $m_{F110W} > 27.85$ mag.

A.6. GRB 060206

GRB 060206 is located at $z = 4.048$ as reported in Fynbo et al. (2006a). We were unable to use TweakReg to align the P60 *R*-band imaging of the afterglow from 2006 February 6 (Ofek et al. 2006) to our HST image due to there being only one sufficiently bright source in common between the two images. We instead align each image separately to the Gaia DR2 catalog. For this alignment, we consider an uncertainty of approximately 1 HST pixel = 0.″065. We detect the afterglow with Source Extractor with a positional uncertainty on the centroid of 0.″016 for a total positional uncertainty of 0.″067. Within a 0.″20 radius region at the position of the afterglow, we detect a source in our HST image. We calculate $P_{cc} = 0.02$ for this galaxy, and we therefore identify it as the host galaxy of this GRB. We measure an apparent magnitude of $m_{F110W} = 27.56 \pm 0.22$ mag.

A.7. GRB 060223

GRB 060223 has a spectroscopic afterglow redshift of $z = 4.406$ as reported by Chary et al. (2007). The only afterglow imaging provided in the literature is *V*-band Swift-UVOT imaging from 2006 February 23 (Blustin et al. 2006). There was only one source (a saturated star) in common between the HST and UVOT images, so we were unable to complete image alignment using TweakReg. Since each image was aligned to Gaia DR2 upon download from their

respective archives, we consider the alignment uncertainty to be within 1 HST pixel = 0.″065. We add this in quadrature to the afterglow centroid uncertainty measured with Source Extractor of 0.″042 to get a total afterglow positional uncertainty of 0.″077. The afterglow position and its 3σ (0.″23) uncertainty region are coincident with a source in the HST image. We calculate $P_{cc} = 0.06$ for this source and identify it as the host galaxy of GRB 060223. We measure an apparent magnitude of this galaxy of $m_{F110W} = 26.63 \pm 0.07$ mag. For this host galaxy, Blanchard & Berger (2016) report a Galactic-extinction-corrected magnitude of $m_{F110W} = 26.534 \pm 0.069$ mag, which is consistent with our measurement of $m_{F110W} = 26.53 \pm 0.07$ mag.

A.8. GRB 060510B

GRB 060510B has a spectroscopic afterglow redshift, $z = 4.941$, as measured in Price et al. (2007). We align *i*-band GMOS-N imaging of the afterglow from 2006 May 10 (Price et al. 2006) to the HST image. We measure an rms alignment uncertainty of 0.″09, and we add this in quadrature to the afterglow centroid uncertainty of 0.″0062 measured with Source Extractor for a total afterglow positional uncertainty of 0.″09. The afterglow position and its 3σ (0.″27) uncertainty region are coincident with a source in the HST image. We calculate $P_{cc} = 0.04$ for this source and identify it as the host galaxy of this GRB. We measure an apparent magnitude of this source of $m_{F110W} = 26.05 \pm 0.06$.

A.9. GRB 060522

GRB 060522 has a spectroscopic afterglow redshift of $z = 5.110$ as reported in Chary et al. (2007). We reduced *R*-band TNG imaging of the afterglow from 2006 May 22 and report a 0.″028 uncertainty on the centroid of the afterglow. We align this reduced image to the HST image and report an uncertainty of 0.″05 on this astrometric alignment. We sum these uncertainties in quadrature and report a total positional uncertainty of 0.″05. We do not detect a source within a 0.″15 radius region centered at this afterglow position in the HST image. We find three sources within a 5″ box centered at the position of the afterglow, and we calculate P_{cc} values for all above 0.2. For this reason we consider the host of this GRB to be a nondetection. We report a limiting magnitude of $m_{F110W} > 27.83$ mag. For this source, Blanchard & Berger (2016) report a nondetection and an upper limit of $m_{F110W} > 28.9$ mag, and Tanvir et al. (2012a) report a nondetection and an upper limit of $m_{F110W} > 28.13$ mag. Blanchard & Berger (2016) define their 3σ upper limits as the magnitude at which sources are detected at 3σ significance. The result from Tanvir et al. (2012a) is inconsistent with our upper limit, however they perform forced photometry in a 0.″4 radius aperture at the afterglow location and also use a 2σ detection threshold. When we apply the same methods, we are able to reproduce their limit. For consistency of our GRB host galaxy sample, we continue with our limit of $m_{F110W} > 27.83$ mag.

A.10. GRB 060927

GRB 060927 has a spectroscopic afterglow redshift of $z = 5.467$ as detailed in Ruiz-Velasco et al. (2007) from VLT/FORS1 spectroscopy. We are unable to find the centroid of the afterglow with Source Extractor due to blending with a nearby galaxy in *I*-band VLT imaging at 2.6 days posttrigger (Ruiz-Velasco et al. 2007), but the afterglow is visible in DS9 after adjusting the scale and smoothing parameters. We are able to estimate the center of the afterglow to within 0.5 VLT pixels (0.″126), and we also report a 0.″023 astrometric uncertainty, resulting in a total positional uncertainty of 0.″128 for the afterglow. There are no sources detected within 0.″385 of this position. Within a 5″ box centered at the position of the afterglow, we find three sources and calculate P_{cc} values for two of them above 0.8. The third source (the only one visible with our scaling choice in Figure 1 and is the blended source in the VLT imaging) had $P_{cc} = 0.11$. This nearby source was detected in VLT *R*-band imaging (Basa et al. 2012) and therefore is at $z < 4$, and we therefore exclude this source as the possible host galaxy for GRB 060927. For these reasons, we consider the host of this GRB to be a nondetection. We report a limiting magnitude of $m_{F110W} > 27.84$ mag. Tanvir et al. (2012a) report a limiting magnitude $m_{F110W} > 28.57$, however they perform forced photometry in a 0.″4 radius aperture at the afterglow location and also use a 2σ detection threshold. When we apply the same methods, we are able to reproduce their limit. For consistency of our GRB host galaxy sample, we continue with our limit of $m_{F110W} > 27.84$ mag.

A.11. GRB 071025

GRB 071025 has a photometric afterglow redshift of $z = 4.8 \pm 0.4$ as presented in Perley et al. (2010). To identify the host galaxy of this GRB, we use *H*-band REM imaging of the afterglow from 2007 August 25. We were successful in using TweakReg to align the afterglow and HST images, despite there being few sources (many of them saturated stars) in common between the fields. We report an alignment rms uncertainty of 0.″22 and an afterglow centroid uncertainty of 0.″14 for a total positional uncertainty on the afterglow of 0.″26. We detect one source within 0.″78 of the afterglow position in the HST image, though this source has a calculated $P_{cc} = 0.12$. We identify only one other source within 5″ of the afterglow position: the bright source in the upper left corner in Figure 1. We measure an apparent magnitude of $m_{F110W} = 23.6573$ mag and $P_{cc} = 0.24$ for this source. Because of the bright magnitude and higher P_{cc}, we elect to identify the first source as the host galaxy of GRB 071025. We report an apparent magnitude of $m_{F110W} = 26.06 \pm 0.10$ mag for this galaxy.

A.12. GRB 090516A

GRB 090516A has a spectroscopic afterglow redshift of $z = 4.111$ as reported in de Ugarte Postigo et al. (2012). We identify the afterglow in VLT/FORS2 *R*-band imaging from 2009 May 17 and align this imaging to the HST image of the field of the GRB. We report an astrometric alignment uncertainty of 0.″022 and a centroid positional uncertainty of 0.″0058 for a total positional uncertainty on the afterglow of 0.″023. This position and its 3σ uncertainty region are directly on a galaxy in the HST image. We calculate $P_{cc} = 0.08$ for this source and identity it as the host galaxy of GRB 090516A. We report an apparent magnitude of $m_{F110W} = 25.04 \pm 0.07$ for this galaxy. This source was also identified by Greiner et al. (2015) and has a reported $M_{UV} = -20.99 \pm 0.4$ mag, which is consistent with our absolute magnitude of $M_{UV} = -21.24 \pm 0.07$ mag.

A.13. GRB 100219A

GRB 100219A has a spectroscopic afterglow redshift of $z = 4.667$ as measured in Selsing et al. (2019). We reduce r-band Gemini/GMOS-S images from 2010 February 20 of the afterglow (Cenko et al. 2010a). We align this imaging to the HST image, and we measure an astrometric alignment uncertainty of 0.″017 and a centroid uncertainty of 0.″032 for a total positional uncertainty on the afterglow of 0.″036. We detect no sources within 0.″12 of the afterglow position, and we tentatively classify this as a nondetection for the host galaxy of GRB 100219A. We find two sources within a 5″ box centered at the position of the afterglow. We calculate P_{cc} values of 0.33 and 0.09. The galaxy with $P_{cc} = 0.09$ is the large galaxy to the northeast of the afterglow region in Figure 1. This source is galaxy BN2010[14] at a redshift of $z = 0.217$ as reported in Cenko et al. (2010a), and is therefore not the host galaxy of GRB 100219A. For these reasons, we consider the host of this GRB to be a nondetection. We estimate a limiting apparent magnitude of $m_{F110W} > 27.58$ mag. Thöne et al. (2013) report a 2σ detection of a source at the position of the afterglow in GTC/OSIRIS i-band imaging. They report $m_{i'} = 26.7 \pm 0.5$, which Greiner et al. (2015) convert to $M_{UV} = -19.74 \pm 0.5$ mag. This value is inconsistent with our limiting absolute UV magnitude of $M_{UV} > -18.78$ mag.

A.14. GRB 100513A

GRB 100513A has a redshift of $z = 4.772$ measured from Gemini/GMOS-N afterglow spectroscopy (Cenko et al. 2010b; Tanvir et al. 2019). From R-band GMOS-N imaging from 2010 May 13, we detect the afterglow and report a 0.″0010 uncertainty on the astrometric alignment and a 0.″022 uncertainty on the centroid for a total positional uncertainty on the afterglow of 0.″022. This position and its 3σ uncertainty region are coincident with a source in the HST image. We calculate $P_{cc} = 0.03$ for this source and identity it as the host galaxy of this GRB. We measure an apparent magnitude of $m_{F110W} = 26.65 \pm 0.15$ mag.

A.15. GRB 111008A

GRB 111008A has a redshift of $z = 4.9898$ as measured from VLT/X-shooter afterglow spectroscopy as analyzed in Wiersema et al. (2011). We reduced R-band GMOS-S afterglow imaging from 2011 October 9 and aligned it to the HST image. We report an astrometric alignment uncertainty of 0.″061 and an uncertainty on the centroid of the afterglow of 0.″052. We sum these in quadrature for a total positional uncertainty of 0.″080. We detect a source partially within the 3σ uncertainty region within the HST image. We calculate $P_{cc} = 0.03$ for this source, and we therefore report the first galaxy as the host of this GRB. We measure an apparent magnitude of $m_{F110W} = 27.69 \pm 0.3$ mag. While this source is clearly visible with the standard "zscale" in DS9, we note that we had to lower the Source Extractor detection thresholds from their default values for it to be identified. This apparent magnitude converts to $M_{UV} = -18.71 \pm 0.30$ mag, and it is consistent with the limiting magnitude of $M_{UV} > -20.88$ mag reported in Greiner et al. (2015) and Sparre et al. (2014).

[14] http://simbad.cds.unistra.fr/simbad/sim-id?Ident=%409106632&Name=%5bBN2010%5d%20J101648.52-123357.5&submit=submit

A.16. GRB 120712A

GRB 120712A has a redshift of $z = 4.1745$ as reported in Xu et al. (2012) from a VLT/X-shooter spectrum of the afterglow. We reduce R-band GMOS-S afterglow imaging from 2012 July 12 and align this to our HST image for host identification. We measure an astrometric alignment uncertainty of 0.″058 and an uncertainty on the afterglow centroid of 0.″0064. We therefore report a total positional uncertainty on the afterglow of 0.″058. At the location of the afterglow, we detect a source in the HST image with $P_{cc} = 0.06$, and we identify this source as the host galaxy. We measure an apparent magnitude of $m_{F110W} = 27.06 \pm 0.12$ mag.

A.17. GRB 130606A

GRB 130606A has a redshift of $z = 5.913$, as reported in Lunnan et al. (2013) from MMT/Blue Channel afterglow spectroscopy. We reduce and align i-band Gemini/GMOS-N imaging of the afterglow from 2013 June 7 (Chornock et al. 2013) to our HST/WFC3/F140W image. We report an astrometric alignment uncertainty of 0.″026 and an uncertainty on the centroid of the afterglow of 0.″002. The position of the afterglow is on a source in the HST image, and we calculate $P_{cc} = 0.02$ for this galaxy. We therefore identify this source as the host galaxy of GRB 130606A, in agreement with the host identification of McGuire et al. (2016). We measure an apparent magnitude of $m_{F140W} = 26.79 \pm 0.05$ mag, while McGuire et al. (2016) report $m_{F140W} = 26.34^{+0.14}_{-0.16}$ mag for this source from the same HST images. While our values are inconsistent, when we use the aperture size reported in McGuire et al. (2016), we are able to reproduce their findings. For consistency of our GRB sample, we choose to use our measurement of $m_{F140W} = 26.79 \pm 0.05$ mag for analysis.

A.18. GRB 131117A

GRB 131117A is located at $z = 4.042$, as measured from VLT/X-shooter spectra from Hartoog et al. (2013). We reduce and stack R-band VLT/X-shooter imaging from 2013 November 17 in order to attempt host identification. Due to the poor quality of the afterglow imaging and few sources visible in the frame (<10) including a saturated star and the afterglow, it was not possible to use TweakReg to align the afterglow image to the HST image, however upon visual inspection, the images appear to be aligned to within 1 HST pixel (0.″065). We use Source Extractor to measure an uncertainty on the centroid of the afterglow of 0.″053 for a combined total positional uncertainty on the afterglow of 0.″084. We find no sources in the HST image within 3σ of the afterglow position. We find two sources within a 5″ of this location, and we calculate P_{cc} values for both above 0.7. For this reason we consider the host of this GRB to be a nondetection. We estimate a limiting magnitude of $m_{F110W} > 27.39$ mag at 3σ above background in a 0.″37 radius aperture.

A.19. GRB 140304A

GRB 140304A has a redshift of $z = 5.283$ as measured from GTC/OSIRIS afterglow spectroscopy in Jeong et al. (2014). The radio afterglow of this GRB was well detected with the VLA (Laskar et al. 2014), and we report that position and its uncertainty in Table 1. We do not detect any sources to within

3σ of this afterglow position in the HST image. We find four sources within a 5″ box centered at the position of the afterglow, and we calculate P_{cc} values for all above 0.4. For these reasons, we consider the host of this GRB to be a nondetection. We measure a limiting magnitude for this galaxy of $m_{F110W} > 27.49$ mag.

A.20. GRB 140311A

GRB 140311A has a redshift of $z = 4.954$ as measured from Gemini/GMOS-N spectroscopy of the afterglow (Chornock et al. 2014b). From *i*-band GMOS-N imaging from 2014 March 12 from the same reference, we measure an uncertainty of 0.″058 on the astrometric alignment to the HST image and an uncertainty on the centroid of the afterglow of 0.″016. This results in a total afterglow positional uncertainty of 0.″060. At the location of the afterglow, we detect a source in our HST image with $P_{cc} = 0.03$, and we classify it as the host of GRB 140311A. We measure an apparent magnitudes of $m_{F110W} = 28.38 \pm 0.35$ mag.

A.21. GRB 140428A

GRB 140428A is located at a redshift $z = 4.68^{+0.52}_{-0.18}$ as measured from afterglow photometry reported in Bolmer et al. (2018). We reduced and aligned *I*-band Keck/LRIS imaging from 2014 April 29 (Perley 2014) to our HST image and report an astrometric tie uncertainty of 0.″061. We measure an uncertainty on the centroid of the afterglow of 0.″026 for a total afterglow positional uncertainty of 0.″066. We find no sources in the HST image within 0.″18 of the afterglow position. We find four sources within a 5″ box centered at the position of the afterglow, and we calculate P_{cc} values for all above 0.2. For this reason, we consider the host galaxy of GRB 140428A to be a nondetection, and we report a limiting magnitude of $m_{f110w} > 27.66$ mag.

A.22. GRB 140518A

GRB 140518A is at a redshift of $z = 4.7055$ as reported in Cucchiara et al. (2015) from GMOS-N afterglow spectroscopy. We align *i*-band GMOS-N imaging from 2014 May 18 (Chornock et al. 2014a) to our HST image, and we report an astrometric tie uncertainty of 0.″047. We also report an uncertainty of 0.″002 on the centroid of the afterglow for a total positional uncertainty on the afterglow position of 0.″047. The afterglow position is coincident with a source in the HST image, and we calculate $P_{cc} = 0.05$ for this source. We therefore classify this galaxy as the host of this GRB. We report an apparent magnitude of $m_{F110W} = 27.22 \pm 0.13$ mag.

A.23. GRB 140614A

GRB 140614A has a redshift of $z = 4.233$ as reported in GCN 16401 (Kruehler et al. 2014) from VLT/X-shooter afterglow spectroscopy. We reduce and align *i*'-band VLT/X-shooter imaging of the afterglow from 2014 June 14 (Kruehler et al. 2014) to our HST image and report an uncertainty on this astrometric alignment of 0.″35. We measure an uncertainty of 0.″045 on the centroid of the afterglow with `Source Extractor` for a total positional uncertainty on the afterglow of 0.″349. We detect a source in the HST image within the 3σ uncertainty region. We calculate $P_{cc} = 0.21$. While this is above our threshold of $P_{cc} = 0.1$, we identify this source as the host of this GRB because the source is close to the center of the uncertainty region. We report an apparent magnitude for this galaxy of $m_{F110W} = 26.14 \pm 0.09$ mag.

ORCID iDs

Huei Sears https://orcid.org/0000-0001-8023-4912
Ryan Chornock https://orcid.org/0000-0002-7706-5668
Jay Strader https://orcid.org/0000-0002-1468-9668
Daniel A. Perley https://orcid.org/0000-0001-8472-1996
Peter K. Blanchard https://orcid.org/0000-0003-0526-2248
Raffaella Margutti https://orcid.org/0000-0003-4768-7586
Nial R. Tanvir https://orcid.org/0000-0003-3274-6336

References

Afonso, P., Greiner, J., Pian, E., et al. 2011, A&A, 526, A154
Astropy Collaboration, Price-Whelan, A. M., Lim, P. L., et al. 2022, ApJ, 935, 167
Astropy Collaboration, Price-Whelan, A. M., Sipőcz, B. M., et al. 2018, AJ, 156, 123
Astropy Collaboration, Robitaille, T. P., Tollerud, E. J., et al. 2013, A&A, 558, A33
Barthelmy, S. D., Barbier, L. M., Cummings, J. R., et al. 2005, SSRv, 120, 143
Basa, S., Cuby, J. G., Savaglio, S., et al. 2012, A&A, 542, A103
Bertin, E., & Arnouts, S. 1996, A&AS, 117, 393
Blanchard, P. K., Berger, E., & Fong, W. F. 2016, ApJ, 817, 144
Bloom, J. S., Kulkarni, S. R., & Djorgovski, S. G. 2002, AJ, 123, 1111
Bloom, J. S., Starr, D. L., Blake, C. H., Skrutskie, M. F., & Falco, E. E. 2006, in ASP Conf. Ser. 351, Astronomical Data Analysis Software and Systems XV, ed. C. Gabriel et al. (San Francisco, CA: ASP), 751
Blustin, A. J., Piranomonte, S., Magazzu, A., & Mainella, G. 2006, GCN, 4824, 1
Bolmer, J., Greiner, J., Krühler, T., et al. 2018, A&A, 609, A62
Bouwens, R. J., Illingworth, G., Ellis, R. S., Oesch, P., & Stefanon, M. 2022a, ApJ, 940, 55
Bouwens, R. J., Illingworth, G. D., Oesch, P. A., et al. 2012, ApJL, 752, L5
Bouwens, R. J., Illingworth, G. D., Oesch, P. A., et al. 2014, ApJ, 793, 115
Bouwens, R. J., Illingworth, G. D., Oesch, P. A., et al. 2015, ApJ, 803, 34
Bouwens, R. J., Illingworth, G. D., van Dokkum, P. G., et al. 2022b, ApJ, 927, 81
Bouwens, R. J., Oesch, P. A., Stefanon, M., et al. 2021, AJ, 162, 47
Bradley, L., Sipőcz, B., Robitaille, T., et al. 2023, astropy/photutils: v1.8.0, Zenodo, doi:10.5281/zenodo.7946442
Bunker, A. J., Stanway, E. R., Ellis, R. S., & McMahon, R. G. 2004, MNRAS, 355, 374
Bunker, A. J., Wilkins, S., Ellis, R. S., et al. 2010, MNRAS, 409, 855
Burrows, D. N., Hill, J. E., Nousek, J. A., et al. 2005, SSRv, 120, 165
Cano, Z., Wang, S.-Q., Dai, Z.-G., & Wu, X.-F. 2017, AdAst, 2017, 8929054
Casey, C. M., Scoville, N. Z., Sanders, D. B., et al. 2014, ApJ, 796, 95
Cenko, S. B. 2005, GCN, 3807, 1
Cenko, S. B., Bloom, J. S., Perley, D. A., & Cobb, B. E. 2010a, GCN, 10443, 1
Cenko, S. B., Fox, D. B., Moon, D.-S., et al. 2006, PASP, 118, 1396
Cenko, S. B., Perley, D. A., Morgan, A. N., et al. 2010b, GCN, 10752, 1
Cenko, S. B., Steidel, C., Reddy, N., & Fox, D. B. 2005, GCN, 3366, 1
Chary, R., Berger, E., & Cowie, L. 2007, ApJ, 671, 272
Chevalier, R. A., & Li, Z.-Y. 1999, ApJL, 520, L29
Chornock, R., Berger, E., Fox, D. B., et al. 2013, ApJ, 774, 26
Chornock, R., Fox, D. B., Cucchiara, A., Perley, D. A., & Levan, A. 2014a, GCN, 16301, 1
Chornock, R., Fox, D. B., Tanvir, N. R., & Berger, E. 2014b, GCN, 15966, 1
Ciardi, B., Ferrara, A., Governato, F., & Jenkins, A. 2000, MNRAS, 314, 611
Conselice, C. J., Vreeswijk, P. M., Fruchter, A. S., et al. 2005, ApJ, 633, 29
Covino, S., Piranomonte, S., Fugazza, D., et al. 2007, GCN, 6988, 1
Cucchiara, A., Fumagalli, M., Rafelski, M., et al. 2015, ApJ, 804, 51
Cucchiara, A., Levan, A. J., Fox, D. B., et al. 2011, ApJ, 736, 7
Curran, P. A., Wijers, R. A. M. J., Heemskerk, M. H. M., et al. 2008, A&A, 490, 1047
D'Avanzo, P., & Cummings, J. R. 2006, GCN, 5151, 1
de Ugarte Postigo, A., Fynbo, J. P. U., Thöne, C. C., et al. 2012, A&A, 548, A11
de Ugarte Postigo, A., Gorosabel, J., Malesani, D., Fynbo, J. P. U., & Levan, A. J. 2009, GCN, 9381, 1

Dekel, A., Sarkar, K. C., Birnboim, Y., Mandelker, N., & Li, Z. 2023, MNRAS, 523, 3201
Della Valle, M., Chincarini, G., Panagia, N., et al. 2006, Natur, 444, 1050
Eisenstein, D. J., Willott, C., Alberts, S., et al. 2023, arXiv:2306.02465
Endsley, R., Stark, D. P., Whitler, L., et al. 2023, MNRAS, 524, 2312
Evans, P. A., Beardmore, A. P., Page, K. L., et al. 2009, MNRAS, 397, 1177
Finkelstein, S. L., Bagley, M. B., Ferguson, H. C., et al. 2023, ApJL, 946, L13
Finkelstein, S. L., Papovich, C., Giavalisco, M., et al. 2010, ApJ, 719, 1250
Finkelstein, S. L., Papovich, C., Ryan, R. E., et al. 2012, ApJ, 758, 93
Finkelstein, S. L., Ryan, R. E. J., Papovich, C., et al. 2015, ApJ, 810, 71
Foreman-Mackey, D. 2016, JOSS, 1, 24
Fruchter, A. S., Levan, A. J., Strolger, L., et al. 2006, Natur, 441, 463
Furlanetto, S. R., & Mesinger, A. 2009, MNRAS, 394, 1667
Furlanetto, S. R., & Mirocha, J. 2022, MNRAS, 511, 3895
Fynbo, J. P. U., Starling, R. L. C., Ledoux, C., et al. 2006a, A&A, 451, L47
Fynbo, J. P. U., Watson, D., Thöne, C. C., et al. 2006b, Natur, 444, 1047
Galama, T. J., Vreeswijk, P. M., van Paradijs, J., et al. 1998, Natur, 395, 670
Gal-Yam, A., Fox, D. B., Price, P. A., et al. 2006, Natur, 444, 1053
Gehrels, N., Chincarini, G., Giommi, P., et al. 2004, ApJ, 611, 1005
Gehrels, N., Norris, J. P., Barthelmy, S. D., et al. 2006, Natur, 444, 1044
Gillanders, J. H., Troja, E., Fryer, C. L., et al. 2023, arXiv:2308.00633
Goad, M. R., Tyler, L. G., Beardmore, A. P., et al. 2007, A&A, 476, 1401
Gompertz, B. P., Ravasio, M. E., Nicholl, M., et al. 2023, NatAs, 7, 67
Gonzaga, S., Hack, W., Fruchter, A., & Mack, J. 2012, The DrizzlePac Handbook
Graham, J. F., & Fruchter, A. S. 2013, ApJ, 774, 119
Graham, J. F., Schady, P., & Fruchter, A. S. 2023, ApJ, 954, 21
Greiner, J., Bornemann, W., Clemens, C., et al. 2008, PASP, 120, 405
Greiner, J., Fox, D. B., Schady, P., et al. 2015, ApJ, 809, 76
Han, X. H., Hammer, F., Liang, Y. C., et al. 2010, A&A, 514, A24
Harikane, Y., Nakajima, K., Ouchi, M., et al. 2024, ApJ, 960, 22
Harikane, Y., Ono, Y., Ouchi, M., et al. 2022, ApJS, 259, 20
Harikane, Y., Ouchi, M., Oguri, M., et al. 2023, ApJS, 265, 5
Hartoog, O. E., Xu, D., Malesani, D., et al. 2013, GCN, 15494, 1
Hjorth, J., & Bloom, J. S. 2012, in Gamma-Ray Bursts, ed. C. Kouveliotou, R. A. M. J. Wijers, & S. Woosley (Cambridge: Cambridge Univ. Press), 169
Hjorth, J., Sollerman, J., Møller, P., et al. 2003, Natur, 423, 847
Hook, I. M., Jørgensen, I., Allington-Smith, J. R., et al. 2004, PASP, 116, 425
Jeong, S., Sanchez-Ramirez, R., Gorosabel, J., & Castro-Tirado, A. J. 2014, GCN, 15936, 1
Joye, W. A., & Mandel, E. 2003, in ASP Conf. Ser. 295, Astronomical Data Analysis Software and Systems XII, ed. H. E. Payne, R. I. Jedrzejewski, & R. N. Hook (San Francisco, CA: ASP), 489
Kaplan, E. L., & Meier, P. 1958, J. Am. Stat. Assoc., 53, 457
Kawamata, R., Ishigaki, M., Shimasaku, K., Oguri, M., & Ouchi, M. 2015, ApJ, 804, 103
Kelly, P. L., Filippenko, A. V., Modjaz, M., & Kocevski, D. 2014, ApJ, 789, 23
Kennea, J. A., Burrows, D. N., Hurkett, C. P., Osbourne, J. P., & Gehrels, N. 2005, GCN, 3365, 1
Kennicutt, R. C. J. 1998, ARA&A, 36, 189
Kewley, L. J., Brown, W. R., Geller, M. J., Kenyon, S. J., & Kurtz, M. J. 2007, AJ, 133, 882
Kruehler, T., Vreeswijk, P. M., & Fynbo, J. P. U. 2014, GCN, 16401, 1
Lang, D., Hogg, D. W., Mierle, K., Blanton, M., & Roweis, S. 2010, AJ, 139, 1782
Laskar, T., Berger, E., & Chary, R.-R. 2011, ApJ, 739, 1
Laskar, T., Zauderer, A., & Berger, E. 2014, GCN, 15930, 1
Levan, A., Gompertz, B. P., Salafia, O. S., et al. 2024, Natur, 626, 737
Levan, A. J., Wiersema, K., & Tanvir, N. R. 2011, GCN, 12426, 1
Levesque, E. M., Kewley, L. J., Berger, E., & Zahid, H. J. 2010, AJ, 140, 1557
Lunnan, R., Drout, M., Chornock, R., & Berger, E. 2013, GCN, 14798, 1
Lyman, J. D., Levan, A. J., Tanvir, N. R., et al. 2017, MNRAS, 467, 1795
MacFadyen, A. I., & Woosley, S. E. 1999, ApJ, 524, 262
Madau, P., Haardt, F., & Rees, M. J. 1999, ApJ, 514, 648
Mannucci, F., Cresci, G., Maiolino, R., Marconi, A., & Gnerucci, A. 2010, MNRAS, 408, 2115
Massey, F. J. 1951, J. Am. Stat. Assoc., 46, 68
McGuire, J. T. W., Tanvir, N. R., Levan, A. J., et al. 2016, ApJ, 825, 135
McLure, R. J., Dunlop, J. S., Cirasuolo, M., et al. 2010, MNRAS, 403, 960
Metcalfe, N., Shanks, T., Weilbacher, P. M., et al. 2006, MNRAS, 370, 1257
Meurer, G. R., Heckman, T. M., & Calzetti, D. 1999, ApJ, 521, 64
Miceli, D., & Nava, L. 2022, Galax, 10, 66
Mirocha, J., & Furlanetto, S. R. 2023, MNRAS, 519, 843
Oesch, P. A., Bouwens, R. J., Illingworth, G. D., et al. 2010, ApJL, 709, L16
Ofek, E. O., Cenko, S. B., Soderberg, A. M., & Fox, D. B. 2006, GCN, 4691, 1
Oke, J. B., Cohen, J. G., Carr, M., et al. 1995, PASP, 107, 375
Ono, Y., Ouchi, M., Harikane, Y., et al. 2018, PASJ, 70, S10
Overzier, R. A., Heckman, T. M., Wang, J., et al. 2011, ApJL, 726, L7
Paczynski, B. 1986, ApJL, 308, L43
Palmerio, J. T., Vergani, S. D., Salvaterra, R., et al. 2019, A&A, 623, A26
Peng, C. Y., Ho, L. C., Impey, C. D., & Rix, H.-W. 2010, AJ, 139, 2097
Perley, D. A. 2014, GCN, 16180, 1
Perley, D. A. 2019, PASP, 131, 084503
Perley, D. A., Bloom, J. S., Klein, C. R., et al. 2010, MNRAS, 406, 2473
Perley, R. A., Chandler, C. J., Butler, B. J., & Wrobel, J. M. 2011, ApJL, 739, L1
Perley, D. A., Krühler, T., Schulze, S., et al. 2016a, ApJ, 817, 7
Perley, D. A., Levan, A. J., Tanvir, N. R., et al. 2013, ApJ, 778, 128
Perley, D. A., Tanvir, N. R., Hjorth, J., et al. 2016b, ApJ, 817, 8
Price, P. A., Cenko, S. B., & Fox, D. B. 2006, GCN, 5101, 1
Price, P. A., Songaila, A., Cowie, L. L., et al. 2007, ApJL, 663, L57
Rastinejad, J. C., Gompertz, B. P., Levan, A. J., et al. 2022, Natur, 612, 223
R Core Team 2023, R: A Language and Environment for Statistical Computing, R Foundation for Statistical Computing, Vienna, Austria, https://www.R-project.org/
Robertson, B. E., Ellis, R. S., Furlanetto, S. R., & Dunlop, J. S. 2015, ApJL, 802, L19
Roming, P. W. A., Kennedy, T. E., Mason, K. O., et al. 2005, SSRv, 120, 95
Ruiz-Velasco, A. E., Swan, H., Troja, E., et al. 2007, ApJ, 669, 1
Sahu, K. 2021, WFC3 Data Handbook v5.0 (Baltimore: STScI), https://hst-docs.stsci.edu/wfc3dhb
Salvaterra, R., Campana, S., Vergani, S. D., et al. 2012, ApJ, 749, 68
Savaglio, S., Glazebrook, K., & Le Borgne, D. 2009, ApJ, 691, 182
Schechter, P. 1976, ApJ, 203, 297
Schlafly, E. F., & Finkbeiner, D. P. 2011, ApJ, 737, 103
Schneider, B., Le Floc'h, E., Arabsalmani, M., Vergani, S. D., & Palmerio, J. T. 2022, A&A, 666, A14
Schulze, S., Chapman, R., Hjorth, J., et al. 2015, ApJ, 808, 73
Selsing, J., Malesani, D., Goldoni, P., et al. 2019, A&A, 623, A92
Shen, X., Vogelsberger, M., Boylan-Kolchin, M., Tacchella, S., & Kannan, R. 2023, MNRAS, 525, 3254
Shibuya, T., Ouchi, M., & Harikane, Y. 2015, ApJS, 219, 15
Sparre, M., Hartoog, O. E., Krühler, T., et al. 2014, ApJ, 785, 150
Stan Development Team 2024, RStan: the R interface to Stan. R package v2.32.6, https://mc-stan.org
Stanek, K. Z., Gnedin, O. Y., Beacom, J. F., et al. 2006, AcA, 56, 333
Stark, D. P. 2016, ARA&A, 54, 761
Steidel, C. C., Giavalisco, M., Pettini, M., Dickinson, M., & Adelberger, K. L. 1996, ApJL, 462, L17
Stephens, M. A. 1974, J. Am. Stat. Assoc., 69, 730
Svensson, K. M., Levan, A. J., Tanvir, N. R., Fruchter, A. S., & Strolger, L. G. 2010, MNRAS, 405, 57
Takeuchi, T. T., Yuan, F.-T., Ikeyama, A., Murata, K. L., & Inoue, A. K. 2012, ApJ, 755, 144
Tanvir, N. R., Fynbo, J. P. U., de Ugarte Postigo, A., et al. 2019, MNRAS, 483, 5380
Tanvir, N. R., Le Floc'h, E., Christensen, L., et al. 2021, ExA, 52, 219
Tanvir, N. R., Levan, A. J., Fruchter, A. S., et al. 2012a, ApJ, 754, 46
Tanvir, N. R., Levan, A. J., & Krogsrud, D. 2012b, GCN, 13458, 1
Terry, M. T., & Patricia, M. G. 2000, Modeling Survival Data: Extending the Cox Model (New York: Springer)
Therneau, T. M. 2024, A Package for Survival Analysis in R." R package v3.5-8, https://CRAN.R-project.org/package=survival
Thöne, C. C., Fynbo, J. P. U., Goldoni, P., et al. 2013, MNRAS, 428, 3590
Trenti, M., Perna, R., & Jimenez, R. 2015, ApJ, 802, 103
Treu, T., Roberts-Borsani, G., Bradac, M., et al. 2022, ApJ, 935, 110
Troja, E., Fryer, C. L., O'Connor, B., et al. 2022, Natur, 612, 228
van der Burg, R. F. J., Hildebrandt, H., & Erben, T. 2010, A&A, 523, A74
Vergani, S. D., Palmerio, J., Salvaterra, R., et al. 2017, A&A, 599, A120
Vergani, S. D., Salvaterra, R., Japelj, J., et al. 2015, A&A, 581, A102
Wainwright, C., Berger, E., & Penprase, B. E. 2007, ApJ, 657, 367
Wei, J., Cordier, B., Antier, S., et al. 2016, arXiv:1610.06892
Werner, M. W., Roellig, T. L., Low, F. J., et al. 2004, ApJS, 154, 1
White, N. E., Bauer, F. E., Baumgartner, W., et al. 2021, Proc. SPIE, 11821, 1182109
Wiersema, K., Flores, H., D'Elia, V., et al. 2011, GCN, 12431, 1
Wilkins, S. M., Bunker, A., Coulton, W., et al. 2013, MNRAS, 430, 2885
Woosley, S. E. 1993, ApJ, 405, 273
Woosley, S. E., & Bloom, J. S. 2006, ARA&A, 44, 507
Xu, D., Fynbo, J. P. U., D'Elia, V., & Tanvir, N. R. 2012, GCN, 13460, 1